Chapter 9

Beam Instrumentation

9.1 Overview

This chapter discusses system design of beam instrumentation in SuperKEKB. Table 9.1 summarizes main instrumentation to be installed in SuperKEKB rings. Beam position monitors (BPMs) , 466 in HER and 444 in LER, will be located next to every quadrupole magnets. Signal detecters of the BPM system will be super-heterodyne detectors, turn-by-turn log-ratio detectors with a fast gate which selects one bunch signal, and a detector for BPMs in orbit feedback system which maintains stable collision. Extraction mirrors made of diamond bonded by gold will be prepared for visible photon monitors to reduce the heat deformation by synchrotron light. New X-ray beam profile monitors based on the coded aperture imaging method will be installed for bunch by bunch measurement of the beam profile. A large angle beamstrahlung monitor near the interaction point (IP) will measure the polarization of light generated by the beamstrahlung to obtain information about the beam-beam geometry. The transverse bunch-by-bunch feedback system will be upgraded using new low noise front-end electronics and new 12-bit iGp digital filters. The longitudinal bunch-by-bunch feedback system, which was not equipped in KEKB, will be installed to damp the coherent longitudinal beam instability due to higher order mode in RF cavities.

Table 9.1: Instrumentation in SuperKEKB rings.

System	Quantity	
	HER	LER
Beam position monitor	466	444
Displacement sensor	110	108
Transverse bunch feedback system	2	2
Longitudinal bunch feedback system	0	1
Visible synchrotron radiation size monitor	1	1
X-ray size monitor	1	1
Beamstrahlung monitor	1	1
Betatron tune monitor	2	2
Longitudinal phase monitor	1	1
Beam loss monitor	200	
Direct current-current transformer (DCCT)	1	1
Current transformer (CT)	1	1
Bunch current monitor	1	1

9.2 Beam Position Monitor System

BPM system in SuperKEKB will maximally use that in KEKB to reduce construction cost. Since BPM chambers in LER will be replaced by new ante-chambers, BPM blocks and button electrodes will be newly designed and fabricated. While the 1GHz narrowband detectors in KEKB will be re-used in SuperKEKB HER, those with 509 MHz detection frequency will be used in SuperKEKB LER to fit the ante-chambers whose cut-off frequency is bellow 1 GHz. In addition to the narrowband detectors, 270 gated turn-by-turn detectors will be installed to measure optics function during collision operation. Button electrodes, a wideband detector, a processor unit and a controller for power supplies of actuators will be developed for orbit feedback system to keep the stable collision.

9.2.1 Button Electrode and BPM Chamber

While BPM chambers and button electrodes in KEKB HER will be mostly re-used in SuperKEKB, those in SuperKEKB LER will be newly fabricated. A button electrode has been developed to fit the ante-chamber in LER as

Figure 9.1: BPM electrode for SuperKEKB.

shown in Figure 9.1[2].

A diameter of the electrode is 6 mm to reduce the beam power at the electrode. The electrode is a flange type for easy replacement on troubles and for detachment from the chamber during the TiN coating process on the chamber wall. A pin-type inner conductor ensures tight electrical connection. The estimated longitudinal loss factor of the beam chamber with four electrodes is 0.16 mV/pC. The coupling impedance is 2Ω at the center frequency of 14.8 GHz and the Q value is 38. The estimated growth time of the longitudinal coupled-bunch instability is slower than 120 ms at the maximum beam current, which is much longer than the radiation damping time of 43 ms. A prototype of the electrode was successfully tested at KEKB.

BPMs closest to IP will be located between IP and the final focusing quadrupole magnets. These BPMs are important because they measure beam position without influence of focussing by strong magnets around IP. Since the output power from the beam at these BPMs are much larger than that at the normal BPM due to small inner-diameter of the vacuum chamber of 20mm, a special feedthrough has been designed as shown in Fig. 9.2. The

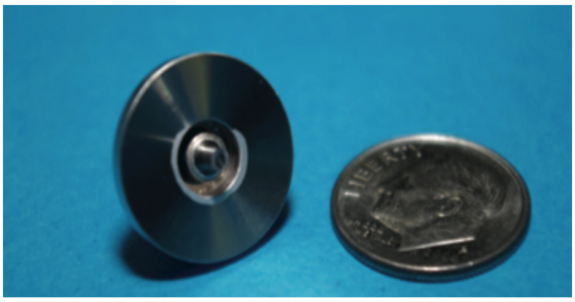

Figure 9.2: Electrode for beam position monitors at closest to collision point.

button head is a simple rod with diameter of 1.8 mm to reduce the power from the beam. The sealing and supporting ceramics is made of silicon nitride with the dielectric constant of 7.9. It has smaller dielectric loss than alumina ceramics. The body and the rod are made of titanium and blazed to a flange made of CuNi. The button signal was simulated using HFSS and GdfidL. The frequency response shows that the trapped modes around the head and ceramics have well higher frequency than that of beam spectrum. The impedance was also estimated from the wake simulation with GdfidL. The shunt impedance of the coupling impedance is 0.3Ω and the Q value is 200 at 14.3 GHz. With the maximum beam current of 3.8 A, estimated power level at 508 MHz is around 6 dBm and estimated total power from beam is around 10W, which is similar level as that at the feedthrough of BPMs near IP in KEKB where both beams in HER and LER pass through the same BPM chamber with large horizontal offset.

BPM chambers made of aluminum for LER are designed by the KEKB vacuum group. A schematic drawing of the BPM chamber is shown in Fig. 9.3[3].

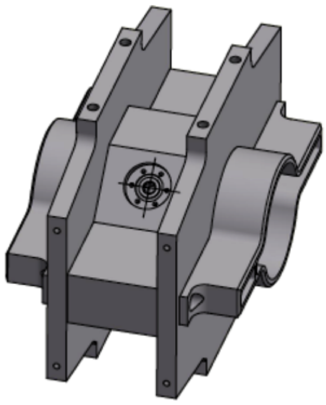

Figure 9.3: BPM chamber in the arc sections in the LER.

9.2.2 BPM detectors

The main BPM detector system in SuperKEKB will follow that in KEKB. The detector in KEKB was a 1 GHz narrowband super-heterodyne detector module accommodated in a VXI main frame[1] . One module covered four BPMs by multiplexing the signals with a switch module. While the narrowband detectors in KEKB will be re-used in SuperKEKB HER, a new narrowband detector with detection frequency of 509 MHz will be used in SuperKEKB LER, since the cutoff frequency of the new ante-chamber is below 1 GHz, i.e. 990MHz. In addition to the narrowband detectors, turn-by-turn detectors with a fast gate will be installed at selected BPMs at the rate of three per betatron wavelength so as to measure the optics during collision. A wideband detector will be introduced at four BPMs closest to IP for orbit feedback to maintain the stable collision. Eight commercial signal processors will be installed for the measurement of orbit oscillation around IP and fast orbit interlock in order to protect extraction windows for aborted beam.Two longitudinal phase monitors, which are re-use of KEKB, will be installed for injection tuning.

Table 9.2 is a list of the detectors in SuperKEKB.

Table 9.2: Detectors for BPM System in SuperKEKB.

Type	Resolution(μm)	Repetition(Hz)	Number of units
Narrowband in KEKB	2	0.25	117
New narrowband	2	0.25	127
Turn-by-turn	50 - 100	100k	270
IR feedback	1	5k	4
Orbit interlock	100	100k	4
Fast oscillation monitor	5	10k to 100k	4
Longitudinal phase monitor	10	100k	2

Narrowband Detector

A 509 MHz narrowband detector which meets the VXI standards is developed based on the 1GHz narrowband detector in KEKB[4]. A schematic diagram of the detector is shown in Fig. 9.4. A selector and a variable

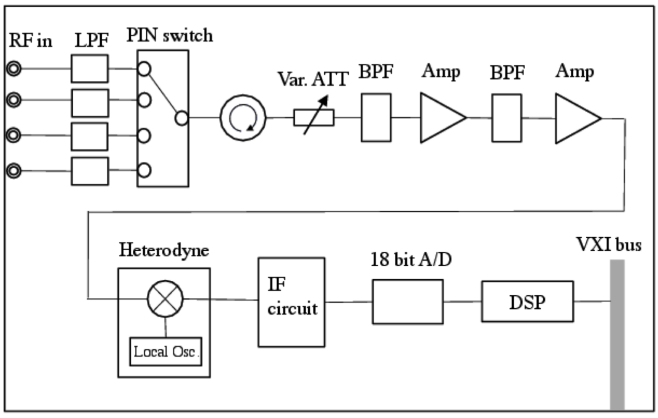

Figure 9.4: 509 MHz narrowband detector[4].

attenuator use PIN-diodes which are directly connected each other without decoupling capacitors. The isolation between channels in the selector is better than 100dB. Its insertion loss is about 1.5dB. An isolator is put between the PIN switch selector and the variable attenuator to reduce the apparent shift of beam position caused by impedance mismatch between the selector and the attenuator. Local signal for a mixer is generated with a high precision synthesizer and a high precision crystal oscillator to reduce phase noise. Polyethylene capacitors are used in the IF(intermediate frequency) circuit to reduce temperature drift.

Achieved signal to noise ratio of B/A, C/A and D/A, where A to D are voltages detected at four channels, is larger than 90dB in a laboratory test with CW as shown in Fig. 9.5.

Gated turn-by-turn detector

The newly developed gated turn-by-turn detectors[5] will be introduced in SuperKEKB. The detector measures the orbit oscillation of a pilot bunch

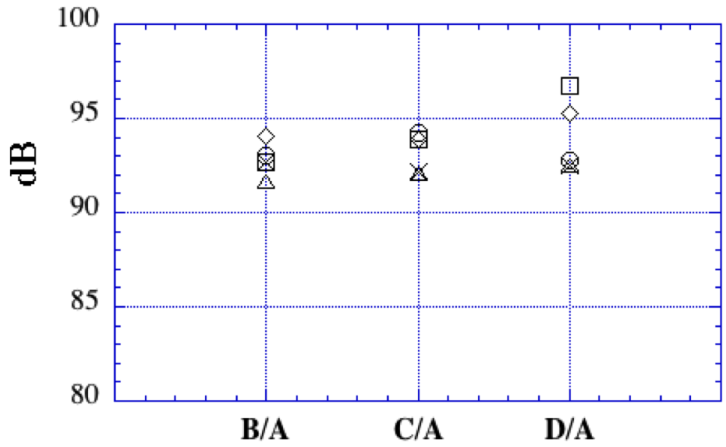

Figure 9.5: Signal to noise ratio normalized by a signal level of the electrode A at the temperature of 20 degrees. The data of five detectors are shown.

at selected BPMs using fast gate, where the pilot bunch is "a non-colliding bunch" located at the end of a bunch train. It also measures the beam orbit of injected beam with small bunch current. About 110 detectors will be installed in the early stage of commissioning. In the future, they will be added depending on the budget.

Since the detector will be inserted between the BPM heads and the narrowband detectors, it should fulfill the following characteristics:

- It should not disturb the measurement of narrowband detectors very much. Noise from the detector, especially switching noise from the fast gate should be suppressed as much as possible.
- The rise and fall time of the gate need to be short enough in order to distinguish the bunch signals with the minimum bunch separation of 4 ns. Also isolation to the turn-by-turn line should be large enough not to be affected by the large power (70dB larger) coming from bunches.
- The system should be compact, all-in-one package to save the mounting space and the fabrication cost.

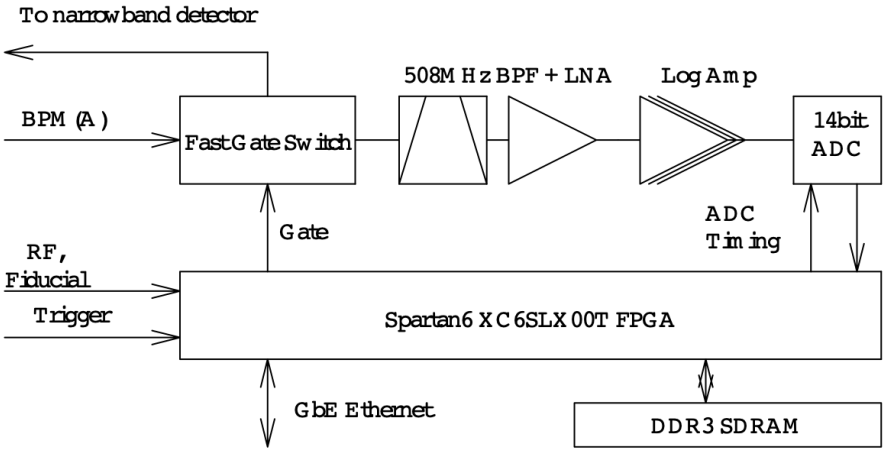

Figure 9.6: Block diagram of the gated turn-by-turn detector.

The block diagram of the gated turn-by-turn detector is shown in Fig. 9.6. It has four independent channels corresponding to four BPM electrodes. Each channel has a fast gate switch, 508 MHz band-pass filters (BPF), low noise amplifiers (LNA, HMC616) with total gain of 40 dB, a logarithmic amplifier (ADL5513), a peak-holding circuit with input to reset timing, and a 14 bit ADC (ADS850). All the timing generation and the data processing are done by a Spartan-6 FPGA (XC6SLX100T-3FGG484) with a 128 MB DDR3 SDRAM. The data and the command is transferred through Gigabit Ethernet interface. The system is installed in a box with 1U size.

A Hittite HMC232LP4 is selected as a SPDT IC. As the measured switching noise is large, typically 70 mV peak to peak, and the isolation less than 67 dB is not so good, we employ a switching-noise cancelling method[6] which combines four SPDT ICs and three 180-deg hybrids as shown in Fig. 9.7. The switching noise is subtracted using two pairs of a 180- deg hybrid, while BPM signal is summed with the same polarity to reduce the insertion loss. For the turn-by-turn measurement, two stages of the SPDT switch are used to enhance the isolation. According to the measurement by a developed module the measured noise is well suppressed down to 2 mVp-p in both channels. The rise and fall response is about 0.6 ns and is short enough for bunch separation of 4 ns. The measured insertion loss and the isolation to narrowband channel around 508 MHz is 2.7 dB and 63 dB, respectively, and those to the turn by turn channel is 4 dB and 80 dB, respectively.

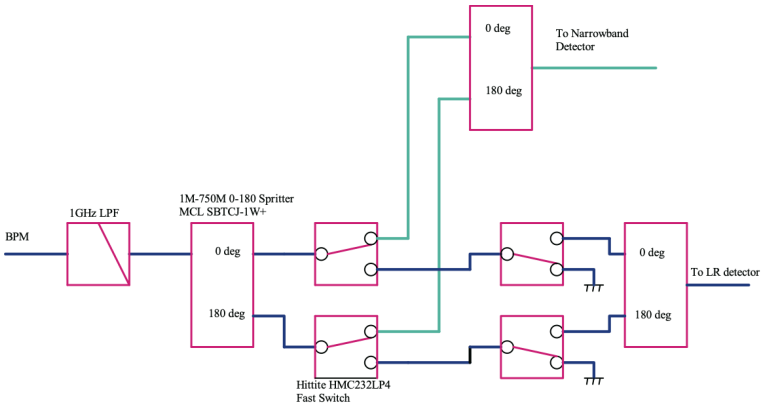

Figure 9.7: Block diagram of the noise-cancelling switch.

The timing jitter was measured using histogram function of a sampling scope with a bandwidth of 20 GHz where the timing of the RF signal and the gate signal was compared. The jitter was around 3.2 ps and the mean timing offset stayed within 20 ps, which is small enough for our purpose.

Giga-bit Ethernet connection is used to control the system. On the Spartan6 FPGA, MicroBlase is used to handle the command from the server. As the large data transfer with the MicroBlase is unacceptably slow, i.e. much slower than 1 MB/s, we implement SiTCP[7] method on the FPGA. Through the SiTCP under GbE connection, data transfer rate amounts to larger than 400 MB/s including the data copy from a DDR3 memory to a FGPA stack.

IP Feedback Detector and Processor Unit

Vertical position at IP of both beams should be controlled by a collision feedback system to maintain stable collision. The four BPMs closest to IP, two in each ring, are used for the IP orbit feedback. The vertical orbit shift at the BPMs by beam-beam deflection is estimated to be several microns. A simulation study shows that the main frequency components of the orbit oscillation due to the vibration of the quadrupole magnets closest to the IP are 25 and 69 Hz.

A special wideband detector for the IP orbit feedback is being developed to measure the orbit at the BPMs[4, 8]. Target performance of the detector is resolution less than 1 μm and repetition rate higher than 5 kHz. The

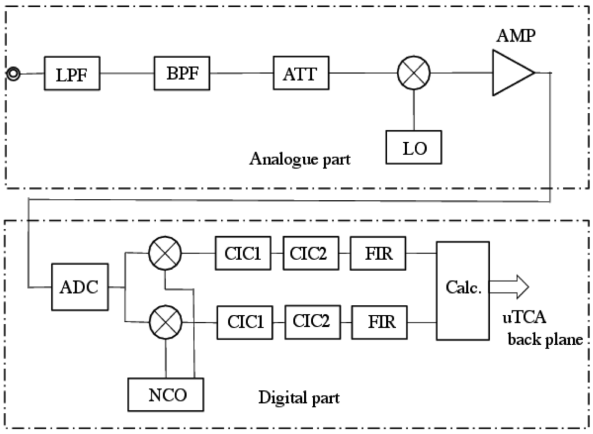

Figure 9.8: IP feedback detector.

schematic diagram of the detector is shown in Fig. 9.8.

The detector converts the 508.8MHz component in BPM signal to an intermediate frequency (IF) of 16.9 MHz with an analog mixer to reduce the degradation of the signal to noise ratio by the clock jitter of an ADC. The IF signal is digitized by the 16 bit ADC with sampling rate of 99.4 MHz, then processed by a chain of digital filters (two CICs and a FIR). The cutoff frequency of the filter is 1 kHz. The digital part is implemented in a micro-TCA board developed for the SuperKEKB LLRF system[9]. A prototype circuit is being tested with CW signal. The jitter of the sampling clock of 1.16ps and the position resolution less than 0.1μm is achieved. The group delay is 1.1 ms for the FIR with 73 taps.

The calculation of the kicks by the correctors will be done by a processor unit based on PID control using the detected beam position[4]. The unit has a FPGA Vertex-5 PowerPC440 on a micro-TCA board as shown in Fig. 9.9. A feedback algorithm is implemented with Matlab/Simulink with system generator from Xilinx for easy coding.

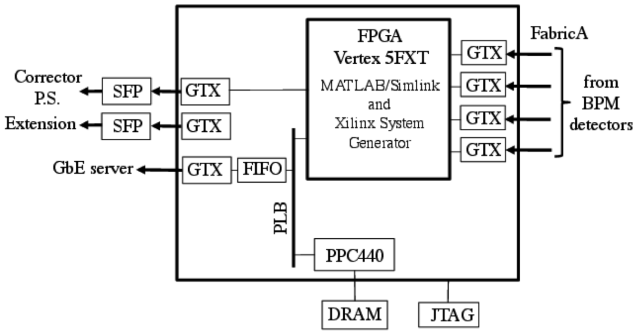

Figure 9.9: Digital Signal Processor for IR feedback[4].

Special purpose detectors

If the beam is aborted while it is oscillating horizontally with large amplitude, the aborted beam may hit outside of the abort window then destroy it. In order to protect the abort window the beam should be aborted if the horizontal orbit exceeds a predetermined level. This interlock system is also useful to protect vacuum components from hit of the beam with large oscillation amplitude. The Libera brilliance+ by Instrumentation Technologies [10] modified for our purpose will be used for this orbit interlock [11]. It continuously monitors the turn-by-turn orbit, then the abort request is asserted in ten turns if the orbit exceeds a predefined interlock level. Fig. 9.10 shows a measurement of interlock latency of a modified Libera brilliance+. Two Libera brilliance+ in each ring will be installed at positions where difference of betatron phase advance is 90 degrees.

Measurement of the beam oscillation is important to get the information of its affect to the luminosity. Also measurement of the beam oscillation at the sextupole magnets, where the vertical beta function is very large in order to correct the chromaticity caused by quadrupole magnets around IP, is important because the vertical orbit deviation at the sextupole magnets

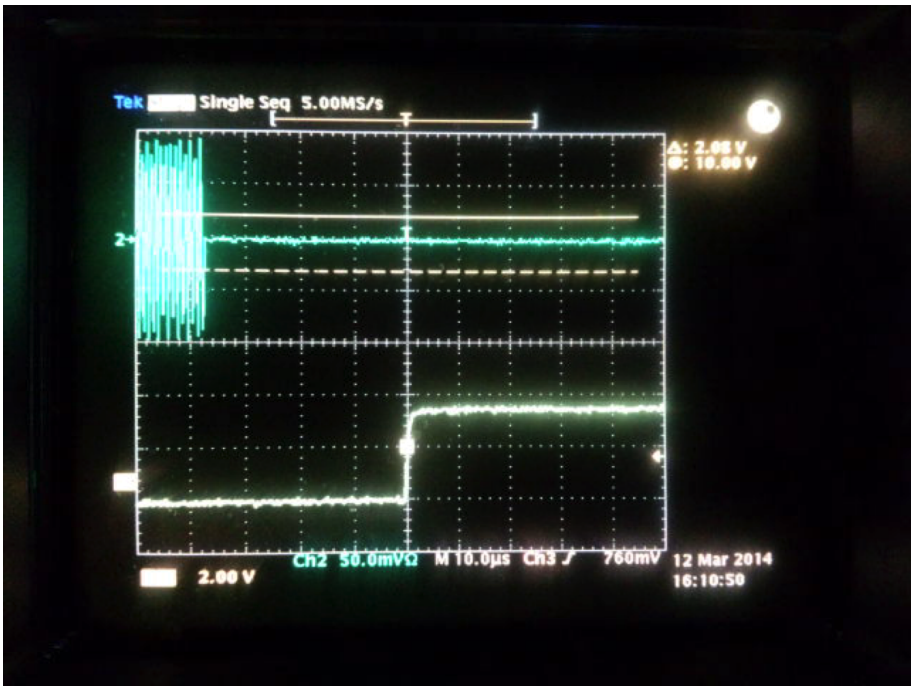

Figure 9.10: A measurement of interlock-latency of a modified Libera brilliance+ processor for orbit interlock. Upper trace is sinusoidal signal supplied to one of input channels of the processor. Lower trace is an interlock signal from the processor. The data shows that the latency is about 40 μs(i.e. 4 turns).

may cause the enlargement of the vertical emitttance or the vertical beam size. For these purposes two Libera brilliance+'s in each ring will be installed at the BPMs near the sextupole magnets (i.e. MQLB1RE and MQLC7RE in HER, MQLB1RP and MQLC3RP in LER) around IP [11].

Two longitudinal phase monitors which measure the longitudinal beam phase with respect to the RF signal will be installed for injection tuning. They are re-use of KEKB.

9.2.3 Displacement sensor

Displacement sensors were introduced in KEKB to measure the mechanical displacement between a BPM head and a neighboring sextupole magnet which was supposed to be caused by deformation of vacuum chambers heated by synchrotron radiation. They will be installed also in SuperKEKB at all BPMs next to the sextupole magnets.

While most displacement sensors will be re-use of KEKB[12], new displacement sensors will be introduced at BPMs next to twenty-four rotatable sextupole magnets installed in the region for the local chromaticity correction around IP at LER, because tolerance for the displacement of the beam at these magnets is tight, 20μm vertically and 40μm horizontally. A sensor support made of MMC (Metal Matrix Composite) which is made of SiC (Silicon Carbide) ceramics and silicon metal and has small coefficient of thermal expansion of 3 10^{-6} /K, is being developed for the new sensor in order to reduce the systematic measurement error due to the thermal expansion of the sensor supports as shown in Fig. 9.11.

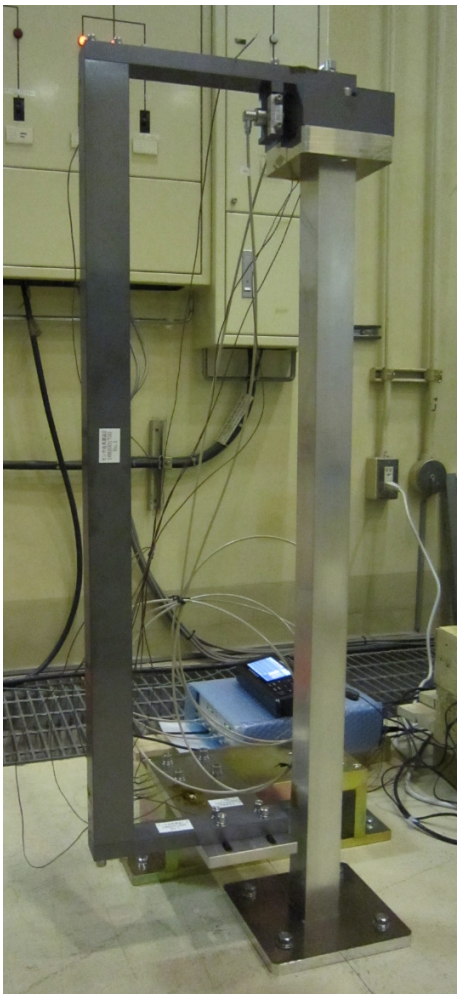

Figure 9.11: A prototype of a sensor support of a BPM displacement sensor made of Metal Matrix Composite. Parts in gray are made of MMC. A sensor target made of MMC is mounted on a silver aluminum rod. Actually the target will be mounted on a BPM block. A horizontal sensor is seen at the side of the sensor target.

Bibliography

[1] M. Arinaga et al., "KEKB beam instrumentation systems", Nuclear Instruments and Methods in Physics Research A 499 (2003) 100???137.

[2] M. Tobiyama et al., "DEVELOPMENT OF BUTTON ELECTRODES FOR SUPERKEKB RINGS", Proceedings of BIW10, Santa Fe, New Mexico, US, 2010.

[3] "Vacuum System", in this design report.

[4] M. Arinaga et al., "BEAM INSTRUMENTATION FOR THE SUPERKEKB RINGS", in proceedings of IBIC2012, Tsukuba, Japan, 2013, p.6-10.

[5] M. Tobiyama, H.Fukuma, H.Ishii and K.Mori, in proceedings of IBIC2013, Oxford, UK. 2013 MOPF23.

[6] T. Naito, et al., in proceedings of IPAC2013, Shanghai, China, p.506-p.508, (2013)

[7] T. Uchida, IEEE Trans. Nucl. Sci. Vol. 55, No.3, 1631-1637, 2008.

[8] H. Ishii et al., "DEVELOPMENT OF A BEAM POSITION DETECTOR FOR AN ORBIT FEEDBACK SYSTEM IN SuperKEKB", in Proceedings of the 8th Annual meeting of Particle Accelerator Society of Japan, 2011.

[9] T. Kobayashi et al., " PROTOTYPE PERFORMANCE OF DIGITAL LLRF CONTROL SYSTEM FOR SUPERKEKB", in Proceedings of IPAC'12, 3470(2012).

[10] http://www.i-tech.si/

[11] S. Kanaeda et al., " PERFORMANCE EVALUATION OF THE LIBERA BRILLIANCE+ AS A BEAM ORBIT OSCILLATION MONITOR AND A BEAM POSITION INTERLOCK MONITOR IN SUPERKEKB", in Proceedings of the 10th Annual meeting of Particle Accelerator Society of Japan, 2013.

[12] Mitsuhiro Arinaga, John W. Flanagan, Hitoshi Fukuma, Takaaki Furuya, Shigenori Hiramatsu, Hitomi Ikeda, Hitoshi Ishii, Eiji Kikutani, Toshiyuki Mitsuhashi, Kenji Mori, Masaki Tejima, and Makoto Tobiyama, Prog. Theor. Exp. Phys. (2013) 03A007.

9.3 Bunch by Bunch Feedback System

9.3.1 Design Considerations

The machine development on the bunch feedback system during the KEKB operation has shown the growth rates of the rings were around the order of few 100 μs or faster[1]. The main source of the impedance has been estimated to be the electron cloud instability for LER[1, 2, 3], and the fast ion instability for HER. They has been anticipated to play major role also in the SuperKEKB rings. The use of the transverse bunch feedback systems will be essential for the smooth commissioning of the rings.

The effect of the noise in the bunch feedback system during collision has also been measured during KEKB operation[4, 5]. Due to the beam-beam effect, the colliding beam showed very wide frequency response besides the betatron frequency. Reduction of the noise components in the bunch feedback system, especially in the detector part is essential to keep the noise effect lower than the level that affects the beam size at the collision point. The signal coupling between the neighboring bunches should also be suppressed.

Though the betatron tunes at the design stage are not very near to the half integer in both horizontal and vertical planes, it is still near to the half integer which limits the stable maximum gain of the feedback system. We will solve the difficulty by employing the dual feedback loops with the betatron phase response roughly 90° apart on both horizontal and vertical planes.

In KEKB operation, the longitudinal bunch feedback system was not needed thanks to the slower growth rate of the instability in nominal operation mode. However, it is expected that the trapped modes in the ARES cavities might cause longitudinal coupled-bunch instabilities at high beam

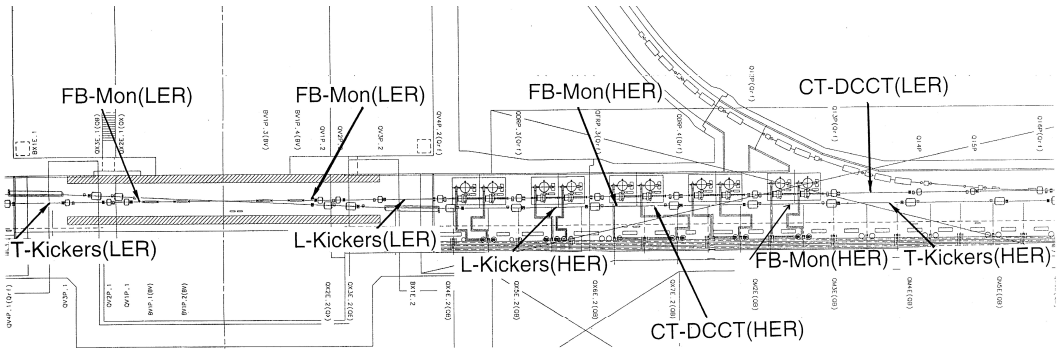

Figure 9.12: Location of the bunch feedback components in SuperKEKB. All the components will be installed at Fuji straight section same as the case of KEKB.

current in LER. We will prepare longitudinal feedback system on LER. For HER, the system is optional because of estimated low growth rate and will not be installed at the start of the beam commissioning.

All the bunch feedback components will be installed in the Fuji straight section as shown in Fig. 9.12. The number of feedback components installed is shown in Table 9.3.

Figure 9.13 shows the block diagram of the transverse and longitudinal feedback systems for SuperKEKB.

Table 9.3: The number of bunch feedback vacuum components installed in Fuji straight section. Parenthesized numbers show future plans.

Component	HER	LER
Bunch position monitor	2	2
Transverse feedback kicker	2	2
Longitudinal feedback kicker	0 (6)	2 (4)

9.3.2 Signal Pickup

We have developed a button electrode with improved impulse response by employing a glass-type sealing with a low relative dielectric constant $\epsilon_r = 4$, as shown in Fig. 9.14[6].

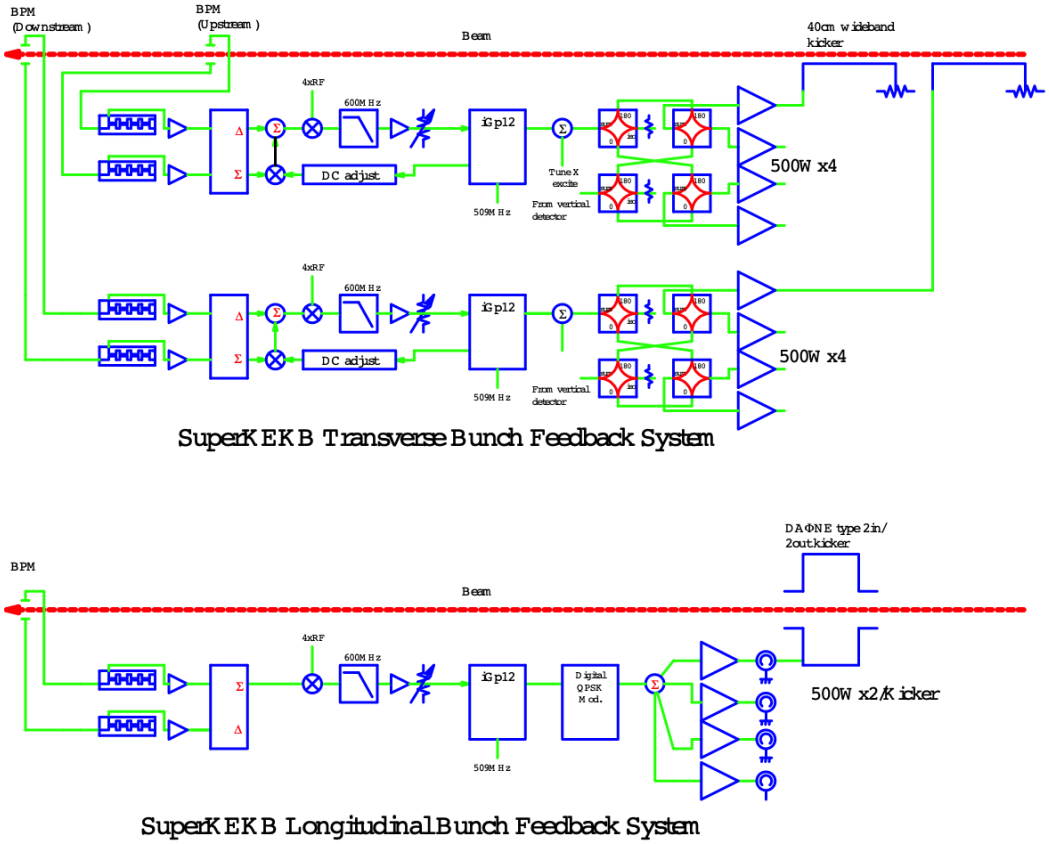

Figure 9.13: Block diagram of the transverse feedback systems (upper) and longitudinal feedback systems (lower) for SuperKEKB.

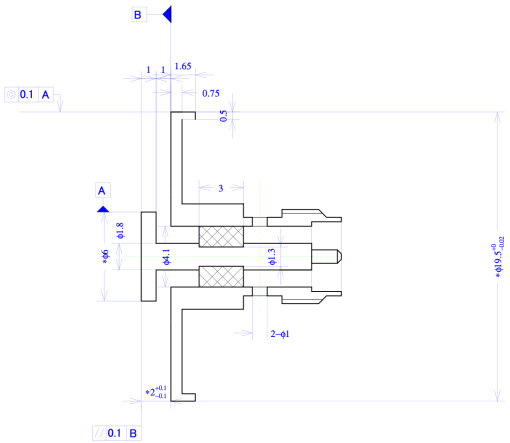

Figure 9.14: Glass-type feedthrough for bunch feedback systems.

The diameter of the button electrode is 6 mm, same as ones used at KEKB. A reverse-type SMA connector with gold-plating is used for the RF output connector. We will attach a 3-dB attenuator directly to the SMA-R connector to reduce the impedance mismatch.

The simulated S-parameter using ANSYS-HFSS[7] is shown in Fig. 9.15.

Twenty four button electrodes (8 horizontal, 8 vertical and 8 between horizontal and vertical planes) will be welded to a circular monitor chamber with inner diameter of 64 mm as shown in Fig. 9.16.

The cutoff frequency of the monitor chamber can be calculated analytically as shown in Table 9.4.

Table 9.4: Cutoff frequency of the monitor chamber.

Mode	Frequency (GHz)
TE11	2.70
TM01	3.53
TE12	4.48

Though the lowest cutoff frequency is higher than 2.5 GHz, we will use the 2 $GHz (= 4 \times f_{RF})$ components of the beam, at least in the early stage of the commissioning, to keep the compatibility with the previous detection system[8, 9]. The GdfidL[10] model of an electrode is shown in Fig. 9.19.

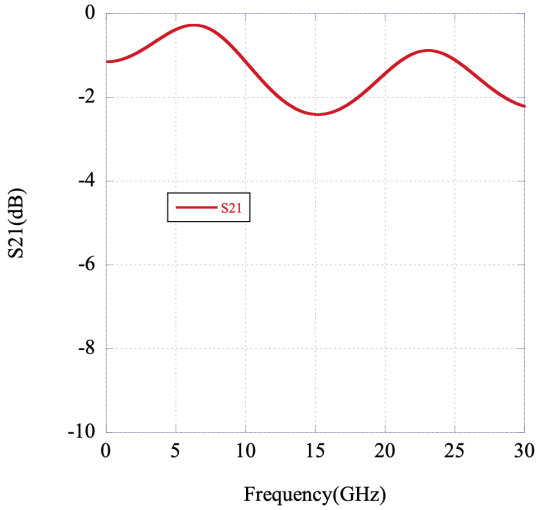

Figure 9.15: Simulated S_{21} of the feedthrough using HFSS.

The simulated output and the coupling impedance for a bunch of $\sigma_z = 6$ mm long is shown in Figs. 9.17, 9.18. The longitudinal loss factor for the bunch length $\sigma_z = 6mm$ is 0.9 mV/pC per four electrodes. The beam response of the electrodes using a short beam at test line of KEK-PF BT from linac has been measured and confirmed to be better than that of ones used at KEKB[6].

9.3.3 Bunch position detection

Figure detect shows the block diagram of the bunch position and bunch charge detectors.

The 2 GHz component ($= 4 \times f_{RF}$) of the signals from the electrode is filtered by the 3-cycles-comb-coupled filter with the center frequency of 2 GHz. Though the insertion loss of the filter is huge, i.e. about 20 dB, the rejection around lower frequency is much larger and the bunch isolation is also much better than that made of a cable-combiner type comb filter. The output of the comb filter is amplified by the wideband low noise amplifier with the noise figure less than 1 dB. For the fine adjustment of the timing between two electrodes, a trombone-delay with maximum stroke of 10 cm is inserted. To make a differential signal and a sum signal from the two inputs, a wideband

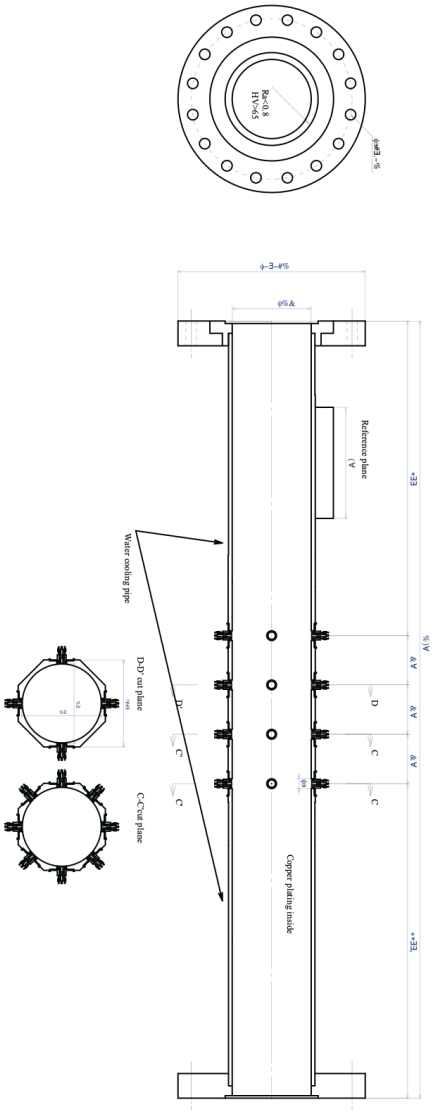

Figure 9.16: Drawing of the HER monitor chamber.

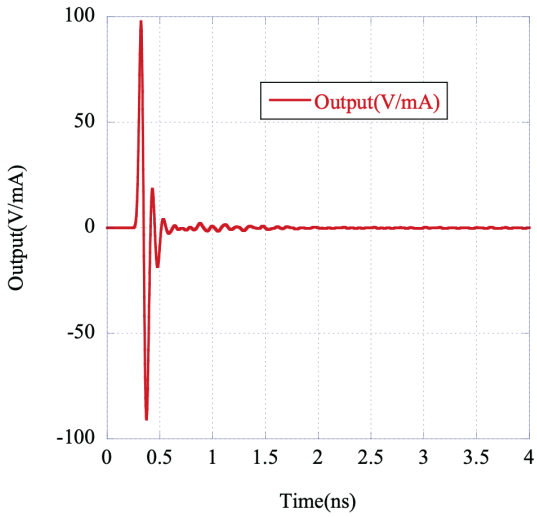

Figure 9.17: Simulated BPM output for 1 mA with $\sigma_z = 6mm$ bunch signal.

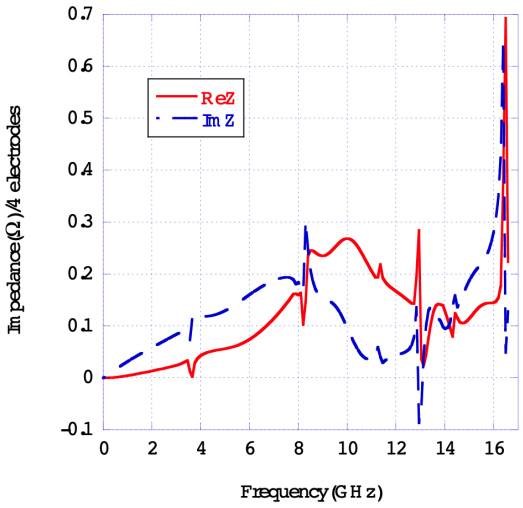

Figure 9.18: Simulated BPM impedance (real part and imaginary part).

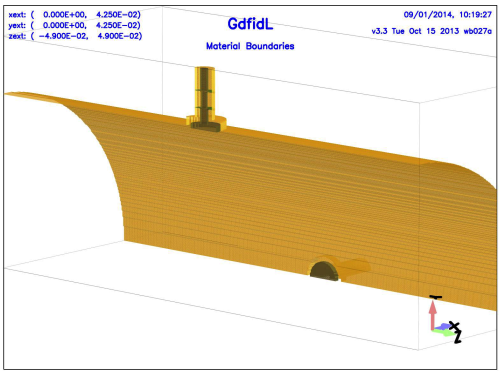

Figure 9.19: GdfidL model of the BPM for the bunch by bunch feedback system.

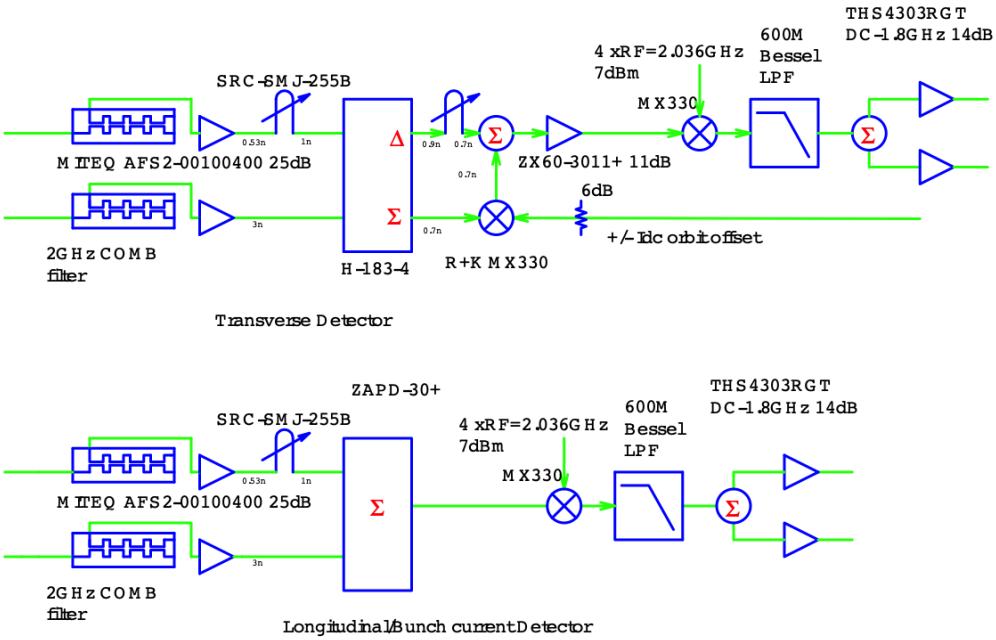

Figure 9.20: Block diagram of the transverse bunch position detector (top) and the longitudinal bunch phase and bunch charge detector (bottom).

Figure 9.21: Picture of the transverse detector.

180-degree hybrid (H-184-3) is used. To cancel the DC components from the difference signal, an amplitude and phase (+ or -) controlled signal-sum is injected with the same timing as the difference signal. The timing between two paths has been tuned using a SRD test pulsar. After the homodyne detection using a double balanced mixer (DBM), the baseband component is filtered by a Bessel type low pass filter with the cutoff frequency of 600 MHz. The output is split into two ways and amplified with DC amplifiers. For the longitudinal detection, we replace the hybrid with a simple wideband power combiner and make a homodyne detection, similar to the transverse detector.

Table 9.5 shows the total number of detectors installed in the local control rack for the bunch by bunch feedback system.

Table 9.5: The number of bunch position detectors.

	HER	LER
Transverse detector	4	4
Longitudinal detector	1	1
Bunch current detector	1	1

Figure 9.21 shows the inside of the transverse detector. The size fits EIA-1U as shown in Fig. 9.22 and has a slide mechanism which enables us to tune the internal components, especially the trombone-delay to adjust the timing difference between two electrodes without dismounting the system.

Figure 9.22: Picture of the transverse and longitudinal detectors installed in a rack.

9.3.4 Signal Processing

The iGp12 digital filters[11] will be used for the signal processing part of the systems. It has 12-bit ADC, 12-bit DAC and 12 Msamples of external recording memory (SRAM). We have received 10 iGp12's in total, 8 of them are with a large Virtex-5 FPGA (VSX95T) and the others are with a normal FPGA (VSX50T). With the normal FPGA, a 10-taps FIR filter is realized, while with the larger FPGA, a 20-taps FIR configuration is available. On the transverse feedback systems, as the time lag coming from the longer FIR filter reduces maximum stable feedback gain especially when the betatron tune is near half or integer tune[12], a 8-taps FIR or a 6-taps FIR filter configuration will be used in real operation. On the other hand for the longitudinal system, a FIR filter with more taps enables us to configure the system without or with small number of down-sampling factor which also limits the maximum stable feedback gain. Though we still need downsampling for $f_s \sim 0.02$ even with a maximum 20-taps FIR filter, we expect the reduction of the downsampling factor enables us larger feedback gain and easier operation.

The following special functions will be implemented in the iGp12s.

- Beam transfer function measurement for a selected bunch.
- Single bunch excitation function using PLL.
  This function enables us to measure the optics function, especially the betatron phase advance between the gated turn-by-turn monitors during the collision.

Figure 9.23: iGp12 digital filters installed in the LER-feedback control room.

We have installed the received iGp12's in the feedback control room as shown in Fig. 9.23 and examined the long-term stability. Some difficulties have already fixed. The current 8-bit iGps will be used as the feedback signal processors for the damping ring and also for the longitudinal phase monitor for HER.

Since we will use the horizontal-vertical combined stripline kickers same as ones used at KEKB, it is necessary to combine two outputs (horizontal and vertical) of the iGp12s. We have developed the active hybrid circuits made with wideband differential amplifiers which pass from DC to nearly 500 MHz signals. The active hybrid circuits will be replaced with the passive RF hybrid circuits used in KEKB.

For the longitudinal modulation, we will continue to use QPSK modulation with the carrier frequency of 1.15GHz($= 2.25 \times f_{RF}$). A digital QPSK modulator has already been developed and has shown excellent performance on the KEK-PF longitudinal feedback system[13].

9.3.5 Power Amplifiers

Transverse amplifiers

To make the dual feedback loop on the transverse plane, we will add four high power feedback amplifiers for each rings. Tables 9.6 and 9.7 show main parameters of the high power amplifiers, including old amplifiers used at KEKB bunch feedback systems.

The amplifiers will be installed on B4 floor under the Fuji crossing bridge

Table 9.6: Main parameters of 500 W transverse feedback amplifiers.

Name	R&K CA010K251-5757R	
No. of available Amps.	12	units
Output polarity	Negative	
Bandwidth	$0.01 \sim 254$	MHz
Gain	> 57	dB
Gain flatness	$\pm$ 2	dB
P_1dB	> 350	W
P_{sat}dB	> 500	W
Input VSWR	< 1.5	
Output VSWR	< 3.0	
Max. Consumption Curr.(200 V)		
at $P_{out} = 500$ W	20	A
Size	$480 \times 650 \times 310$	mm
Weight	70	kg

where almost no radiation is expected. They will be monitored and controlled remotely through GP-IB (R&K amplifiers) or parallel interface (AR amplifiers). As both the pulse response and the maximum power of the CA010K251-5757R amplifiers are much better than the others, we will replace the old amplifiers with CA010K251-5757R after the commissioning. Old 250A250 amplifiers will be used at the bunch feedback systems for the damping ring.

The CA010K251-5757R amplifiers have been tested at the J-PARC MR intra-bunch feedback system with the required bandwidth of 10 kHz $\sim$ 100 MHz and has shown excellent performance. In addition, several minor difficulties have been fixed during the operation.

To protect the transverse amplifiers from beam induced power, we will insert high-power low pass filters (FSY LD 430-7NN-HP) with the cutoff frequency of 300 MHz and the maximum power rating of 1 kW.

Figure 9.24 shows the transverse feedback amplifiers installed at Fuji-B4.

Longitudinal amplifiers

As the carrier frequency of the longitudinal kickers is around 1.14GHz = ($f_{RF} \times 2.25$), we have prepared wideband UHF amplifiers with maximum power of 500 W,

Figure 9.24: Transverse feedback amplifiers 250A250s (left) and CA010K251-5757Rs (right).

Table 9.7: Main parameters of 250 W transverse feedback amplifiers.

Name	AR 250A250	
No. of available Amps.	11	units
Output polarity	Negative	
Bandwidth	$0.01 \sim 250$	MHz
Gain	> 54	dB
Gain flatness	$\pm$ 1.5	dB
P_1dB	> 150	W
P_{sat}dB	> 250	W
Input VSWR	< 1.5	
Output VSWR	< 2.5	
Max. Consumption Curr.(200 V)		
at $P_{out} = 250$ W	7	A
Size	$503 \times 427 \times 551$	mm
Weight	68	kg

as shown in Table 9.8.

In addition to the CA901M182-5757R, we have two sets of MILIMEGA AS0920-500T amplifiers. The parameters of the AS0920-500T amplifiers are similar to those of the CA901M182K-5757R amplifiers, with slightly poor pulse response. Again, all the amplifiers will be installed on the B4 floor under the Fuji crossing bridge as shown in Fig. 9.8 where almost no radiation is expected.

As the longitudinal kicker has no directionality in power, we will install a high power wideband circulator ($P_{max} = 5$ kW, BW 900 MHz $\sim$ 1.8 GHz) and a high power low pass filter of power-consumption type between the amplifier and the kicker.

9.3.6 Transverse feedback kickers

Very similar stripline kickers to those used at the KEKB bunch feedback systems will be used, at the least at the early stage of the commissioning. Table 9.9 shows main parameters of the transverse kickers.

Examples of the drawing and the photo of the transverse stripline kicker are shown in Figs. 9.26, 9.27. The stripline electrode is 40 cm long and made of stainless steel coated with Cu thicker than 10 μm. The downstream

Figure 9.25: Longitudinal feedback amplifiers.

Table 9.8: Main parameters of longitudinal feedback amplifiers.

Name	R&K CA901M182K-5757R	
No. of available Amps.	8	units
Output Polarity	Negative	
Bandwidth	$900 \sim 1800$	MHz
Gain	> 57	dB
Gain flatness	$\pm$ 1.5	dB
P_1dB	> 398	W
P_{sat}dB	> 500	W
Input VSWR	< 2.0	
Output VSWR	< 2.0	
Max. Consumption Curr.(200 V)		
at $P_{out} = 500$ W	25	A
Size	$480 \times 650 \times 265.9$	mm
Weight	68	kg

feedthroughs have bending structure made of BeCu to release thermal expansion due to the heat cycle of the stripline electrode[9]. We have changed the RF connector interface of the kicker from 20D-type to EIA-7/8 type[14], though all the dimensions are completely same except for the fixing hole on the flange.

The longitudinal and transverse impedance and the output of the stripline kicker are simulated using GdfidL. Figures 9.28, 9.29, 9.30, 9.31 show the GdfidL model (1/4), longitudinal impedance, simulated output for $\sigma_z = 6mm$ bunches at the upstream and downstream ports, respectively.

The longitudinal loss factor for $\sigma_z = 6$ mm bunch is 0.185 V/pC.

Figure 9.32 shows the transverse impedance with horizontal offset of 1 mm for the LER stripline kicker.

For higher beam power after phase 3 operation will has started, where maximum beam current of LER will exceed 2 A, we might need better structure tolerant toward much larger power. We will prepare new structure before phase 3 operation with the collaboration of SLAC.

Table 9.9: Main parameters of the transverse feedback kicker.

	HER	LER	
Number of kickers	2	2	
Number of electrodes	4	4	
Inner diameter	104	94	mm
Stripline length	41	41	cm
Stripline angle	60	60	degree
Stripline position from center	39.2	35.2	mm
Stripline thickness	2	2	mm
Stripline characteristic impedance	50	50	Ω
Shunt impedance at lowest freq.	~ 10	~ 10	kΩ
Loss factor	0.176	0.185	V/pC
Kick factor	4.15	5.28	V/pC/m

9.3.7 Longitudinal feedback kickers

We have designed a new longitudinal feedback kicker based on the over-coupled cavity developed at DAFNE[15] to fit our requirement. The basic parameters of the kicker are shown in Table 9.10.

Table 9.10: Basic parameters of the longitudinal feedback kicker.

Input port	2	
Output port	2	
Center Frequency	1.145	GHz
3dB Bandwidth	240	MHz
Shunt Impedance	1.68	kΩ
Longitudinal loss factor	0.406	V/pC /Cavity
Transverse kick factor	2.06	V/pC/m /Cavity
Length (flange-to-flange)	0.44	m

Figures 9.33, 9.34 show the HFSS model and the simulated S-parameter, respectively.

Using GdfidL, we have also estimated the time-domain behavior of the kicker. Figures 9.35, 9.36 and 9.37 show the GdfidL model, estimated longitudinal impedance and port output for $\sigma_z = 6$ mm bunch, respectively.

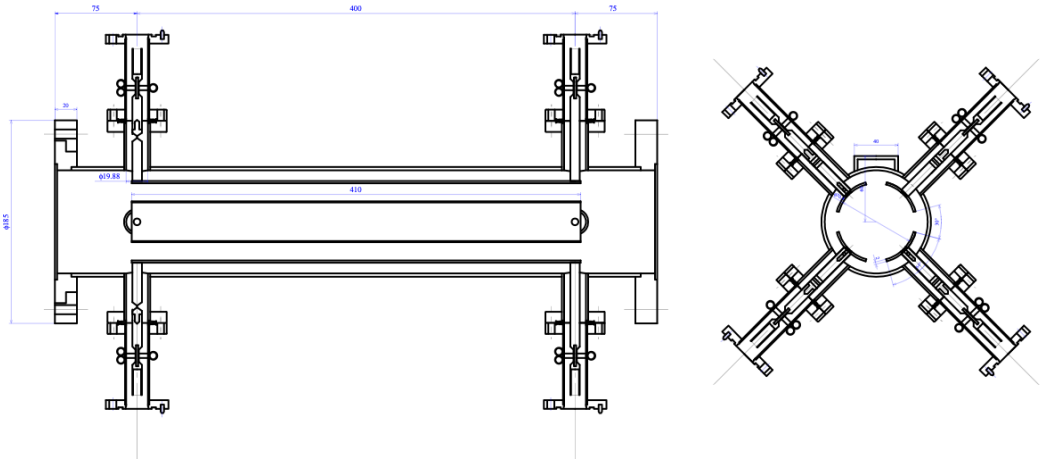

Figure 9.26: Drawing of the LER transverse stripline kicker.

9.3.8 Bunch feedback related systems

We will use the (part of the) bunch feedback systems for the measurement of betatron tunes, bunch current, bunch oscillation and other related measurements such as the beam-beam kick due to collision.

Betatron tune measurement

We will keep the current betatron tune measurement system used at KEKB[8, 9]. There are two systems:

- Global tune measurement system.
  We detect the BPM signal directly using a spectrum analyzer. The output of the tracking generator of the spectrum analyzer is down-converted to baseband signal, and is injected to the feedback loop after the digital filter. We will use this scheme to measure the tunes during the optics correction at low beam current (∼50 mA) where many bunches with fairly small bunch current will exist. The waveform of the spectrum is transferred to EPICS waveform and will be fitted on the optics panel.

- Gated tune measurement system.
  We can excite the non-colliding bunch ("Pilot bunch") not being ap-

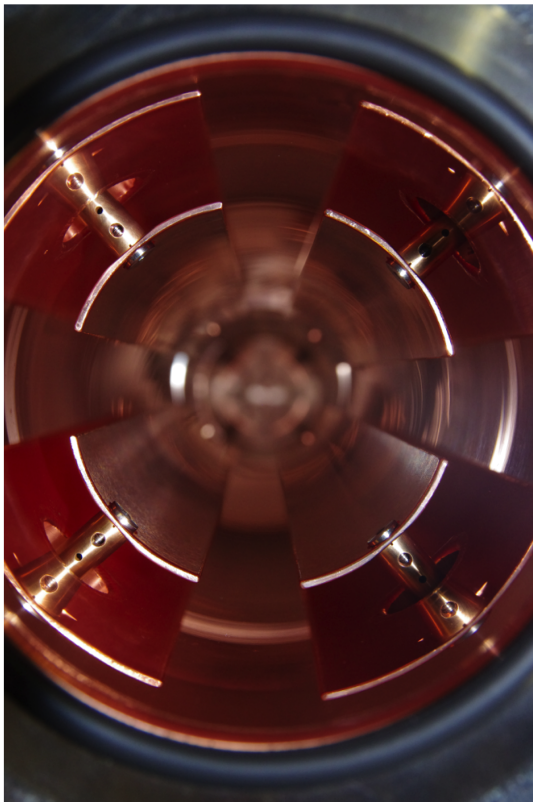

Figure 9.27: Picture of the HER transverse stripline kicker.

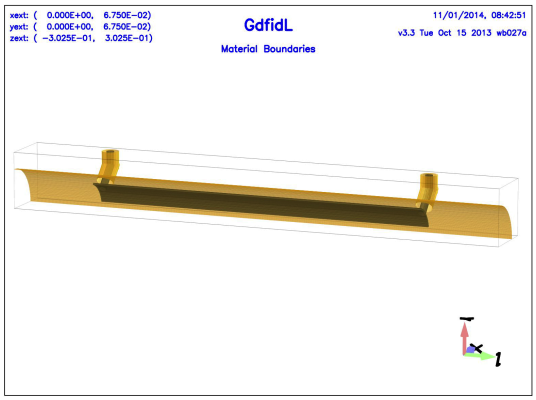

Figure 9.28: GdfidL model of the LER transverse stripline kicker(1/4).

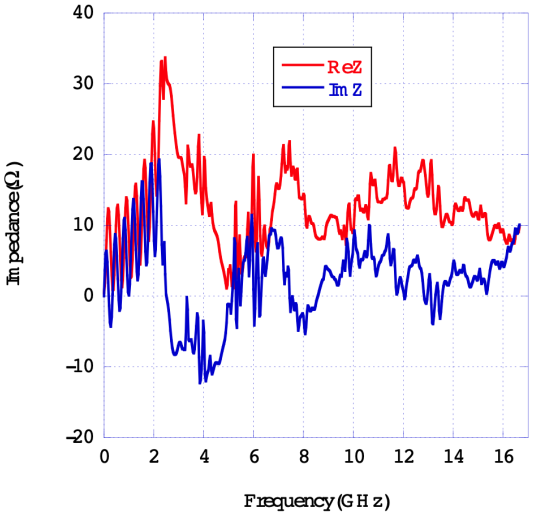

Figure 9.29: Calculated longitudinal impedance of the LER transverse kicker.

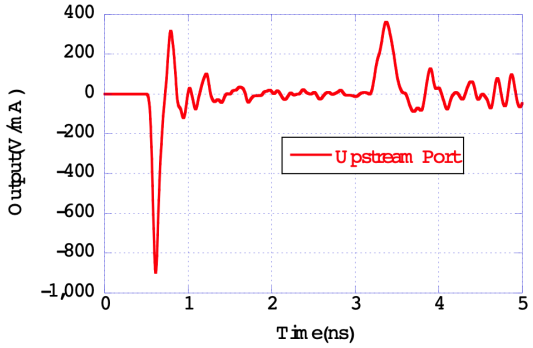

Figure 9.30: Simulated output at upstream port from 1mA/bunch beam.

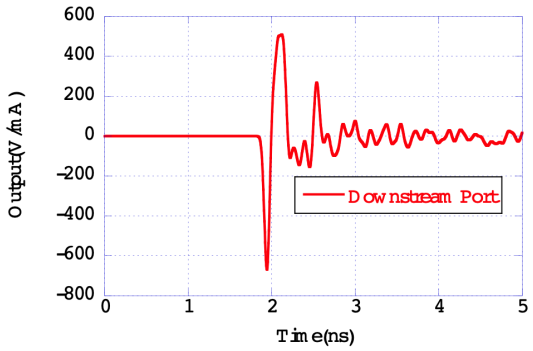

Figure 9.31: Simulated output at downstream port from 1mA/bunch beam.

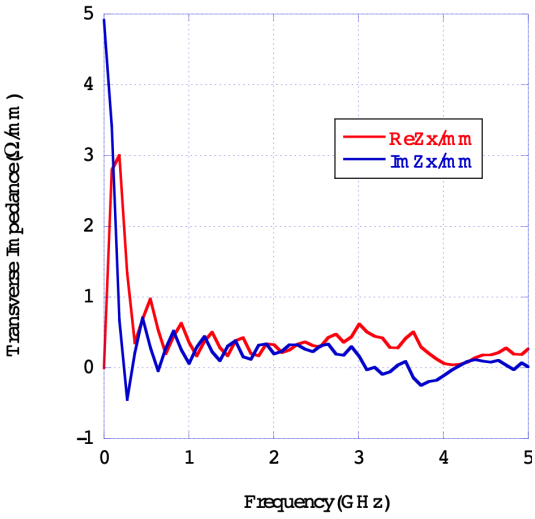

Figure 9.32: Calculated transverse impedance of the LER transverse kicker for the horizontal beam offset of 1 mm.

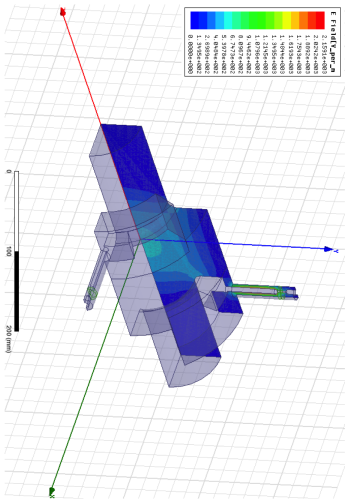

Figure 9.33: HFSS model and simulated E-field magnitude of the longitudinal kicker.

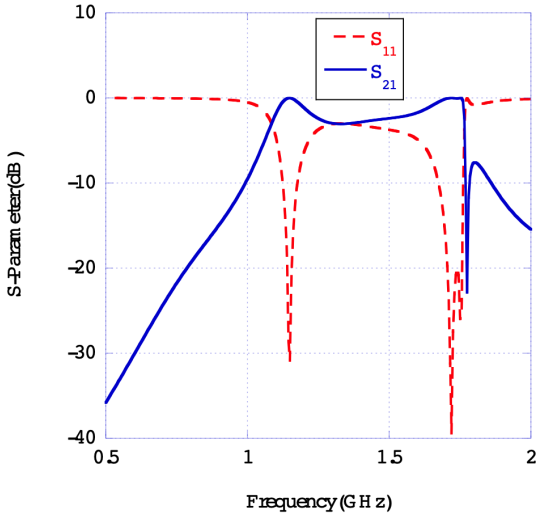

Figure 9.34: Simulated S-parameter using HFSS of the longitudinal kicker.

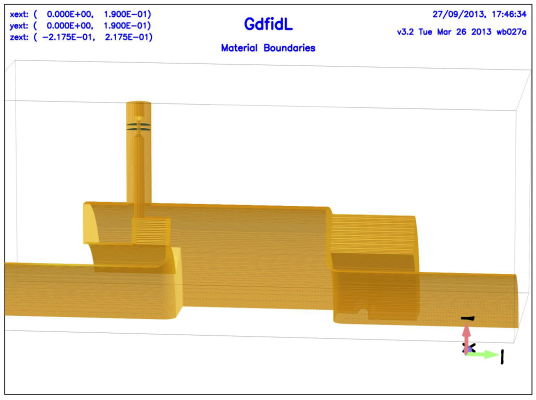

Figure 9.35: GdfidL model of the longitudinal kicker (1/4).

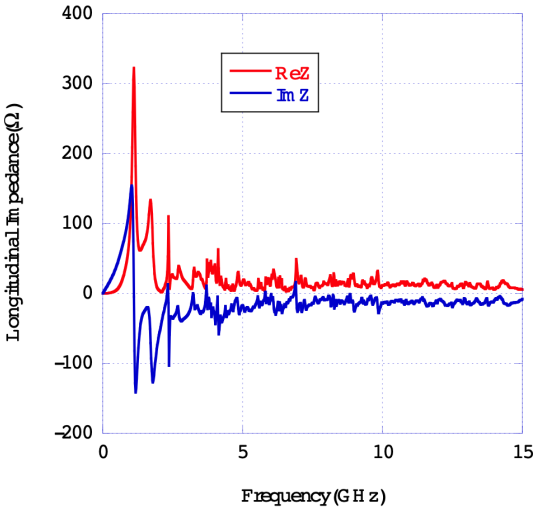

Figure 9.36: Calculated longitudinal impedance of the longitudinal kicker.

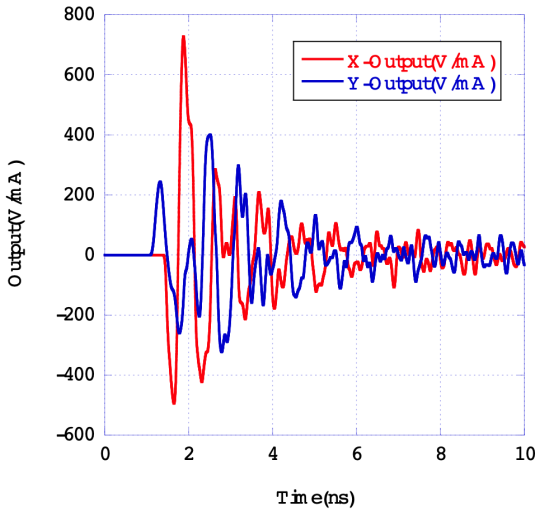

Figure 9.37: Calculated output at the port from $\sigma_z = 6$ mm bunch for the longitudinal kicker.

plied transverse feedback. The system consists of a gated pulsar, single bunch oscillation detection system (BOD) and a spectrum analyzer with a tracking generator. We have used this system to monitor the betatron tune during collision in KEKB. Though we plan to keep the same system, we will omit the analog fast gate to turn off the feedback signal to the pilot bunch– such fast switching will be made in the iGp12 digital filter, if necessary. Moreover, as we will prepare single-bunch betatron oscillation excitation system using PLL-function of the iGp12, this old-fashioned system will be expected to be obsolete soon.

Bunch current monitor

In KEKB, we have measured the bunch current using the bunch feedback techniques (bunch phase detector, hardware two-tap FIR filter, etc.)[16]. We will upgrade the ADC system from old two-taps based system to new system by employing modern technique, such as fast wideband ADC, very fast FPGA and so on. The MAX108 ADC with the bandwidth larger than 1.5 GHz and resolution of 8-bit will be used. The output of the ADC is accumulated using Spartan-6 FPGA. For the bunch current monitor, a block-RAM in the FPGA should be enough even for the KEKB rings. We will also use a huge external

DDR3 memory to measure the longer-time bunch behavior which enable us to replace the old bunch oscillation recorder based on also two-taps FIR filter system to the same ADC system.

Beam-beam kick measurements

We have installed special beam measurement systems using the bunch feedback signal in KEKB to measure special beam behavior such as beam-beam kick or transient beam phase during collision[17, 18]. Very old electronics has been used in this system and it is not easy to keep the function using same modules. We hope to keep this system on SuperKEKB but the resource is fairly limited so the priority for the system is fairly low.

Bibliography

[1] M. Tobiyama, J. W. Flanagan, H. Fukuma, S. Kurokawa, K. Ohmi and S. S. Win, Phys. Rev. ST Accl. Beams **9**, 012801 (2006).

[2] J. W. Flanagan, K. Ohmi, H. Fukuma, S. Hiramatsu, M. Tobiyama, and E. Perevedentsev Phys. Rev. Lett. 94, 054801 (2005).

[3] S. S. Win, K. Ohmi, H. Fukuma, M. Tobiyama, J. W. Flanagan and S. Kurokawa, Phys. Rev. ST Accl. Beams **8**, 094401 (2005)

[4] M. Tobiyama and K. Ohmi, in proceedings of DIPAC2011, Hamburg, Germany, MOPD73.

[5] K. Ohmi, R. Tomas, Y. Funakoshi, R. Calaga, T. Ieiri, Y. Morita, K. Nakanishi, K. Oide, Y. Ohnishi, Y. Sun, M. Tobiyama and F. Zimmerman PRST-AB, **14**, 111003 (2011).

[6] M. Tobiyama, H. Fukuma, K. Shibata, M. Tejima, S. Hiramatsu, K. Mori, H. Ishii, T. Obina, in proceedings of BIW2010, Santa Fe, 2010.

[7] ANSYS HFSS, http://ansys.jp/products/electromagnetics/hfss/

[8] M. Arinaga, J. Flanagan, S. Hiramatsu, T. Ieiri, H. Ikeda, H. Ishii, E. Kikutani , T. Mimashi, T. Mitsuhashi, H. Mizuno, K. Mori, M. Tejima and M. Tobiyama Nucl. Instrum. Meth. Phys. Res. **A499**, p100-137, (2003).

[9] Mitsuhiro Arinaga, John W. Flanagan, Hitoshi Fukuma, Takaaki Furuya, Shigenori Hiramatsu, Hitomi Ikeda, Hitoshi Ishii, Eiji Kikutani, Toshiyuki Mitsuhashi, Kenji Mori, Masaki Tejima, and Makoto Tobiyama, Prog. Theor. Exp. Phys. (2013) 03A007.

[10] http://www.gdfidl.de/

[11] http://www.dimtel.com/

[12] S. Hiramatsu, private communication.

[13] R. Takai, M. Tobiyama, T. Obina, J. W. Flanagan, M. Tadano, T. Mitsuhahi, in proceedings of DIPAC09, Basel, Switzerland, p.59-61, 2009

[14] EIA Standard RS-225.

[15] R. Boni et al., Particle Accelerators 52 (1996) 95-113.

[16] Makoto Tobiyama and Eiji Kikutani Phys. Rev. ST Accl. Beams **3**,012801(2000).

[17] T. Ieiri, K. Akai, H. Fukuma, T. Kawamoto, E. Kikutani, and M. Tobiyama Phys. Rev. ST Accl. Beams **5**,094402(2002).

[18] T. Ieiri, K. Akai, H. Fukuma and M. Tobiyama Nuclear Instruments and Methods in Physics Research **A 606** (2009) 248-256.

9.4 Photon Monitors

We will use two different types of synchrotron radiation (SR) monitors for beam size diagnostics: x-ray monitors and visible-light monitors. The x-ray monitors will be used primarily for vertical bunch profile measurements, and the visible light monitors will be used primarily for horizontal and longitudinal bunch profile measurements, with the possibility of vertical measurements at larger beam sizes for comparison with the x-ray monitor measurements. The collision quality will be monitored using a large-angle beamstrahlung monitor. An energy monitor based on inverse Compton scattering is under consideration for future development, though will not be required at start-up, and is not discussed here.

9.4.1 Visible-light SR monitor

Overview

As at KEKB[1], we will use SR interferometers (using either the horizontal or vertical polarization component) to measure beam sizes from the visible

Table 9.11: Visible SR monitor source parameters.

Parameter	LER	HER	Units
Horizontal emittance ϵ_x	3.20×10^{-9}	4.54×10^{-9}	m
Emittance coupling κ	0.27%	0.25%	
Vertical emittance ϵ_y	8.64×10^{-12}	1.14×10^{-11}	m
Horizontal beta function β_y	8.86	10.17	m
Vertical beta function β_y	30.71	26.92	m
Horizontal beam size σ_y	168	215	μm
Vertical beam size σ_y	16.3	17.5	μm
Beam Energy	4	7	GeV
Bend effective length	0.89	2.90	m
Bend angle	5.04	5.00	mrad
Bend radius ρ	179	580	m
Observation wavelength λ	400	400	nm
SR opening angle $\theta_c(\lambda)$	1.0	0.7	mrad
Hor. slits opening angle α	0.2	0.2	mrad
Ver. slits opening angle α	0.8	0.9	mrad
Required max. measurable hor. visibility γ_{xmax}	90%	90%	
Required max. measurable ver. visibility γ_{ymax}	98%	98%	
Min. measurable hor. beam size σ_{xmin}	164	157	μm
Min. measurable ver. beam size σ_{ymin}	15.7	15.0	μm

component of synchrotron radiation from source bends in the LER and HER. The parameters of the source points are shown in Table 9.11.

When the LER and HER beams have achieved their targeted low emittances, the vertical beam sizes at the monitor source points are below 18 μm in both the LER and the HER. The resolution of the SR interferometer is fundamentally limited by the measurement wavelength λ and the opening angle α between slits as seen from the beam source point, as well as the maximum visibility (fringe modulation) that can be reliably measured; for a Gaussian beam, the beam size σ is given by $\sigma = \frac{\lambda}{\pi(\alpha)}\sqrt{\frac{1}{2}\ln\frac{1}{\gamma}}$. The opening angle is in principle limited by the SR opening angle and by mechanical considerations, with the latter being the dominant restriction at SuperKEKB; the mirrors are located in antechambers to minimize HOM losses, with the height of the antechambers limited by the pole gap of upstream quadrupole magnets to 24 mm in height. The mirrors are located at a distance F of 24.5 (23.5) m downstream of the source point in the LER (HER), so with a maximum effective slit separation D of 20 mm at the mirror location, the slits opening angle $\alpha = D/F$ is 0.8 (0.9) mrad in the LER (HER). For a 400 nm measurement wavelength, it would be necessary to be able to measure visibilities of around 98% to measure the vertical beam sizes at the source points. This would be extremely challenging.

In the horizontal direction, the beam sizes are 10 times or more larger than the vertical ones, so the required measurable maximum visibility is a much more reasonable 90%, assuming 9 mm-wide mirrors.

Accordingly, the visible SR interferometers will primarily be used for horizontal beam size measurements. In the vertical direction, it can still be used at larger beam sizes for cross-calibration with the x-ray beam size monitor.

The SR interferometer will not be capable of single-bunch, single-shot measurements, only integrated ones over many turns of the whole beam, due to limited photon statistics at shorter integration times.

The longitudinal bunch profiles will be measured by streak-cameras.

Extraction mirrors

Beryllium mirrors used at KEKB suffered from heat distortion due to absorbed SR power, which caused the apparent beam size to change as a function of beam current. The synchrotron radiation monitors at SuperKEKB

Table 9.12: Visible SR monitor source point power.

	KEKB		SuperKEKB		
Parameter	LER	HER	LER	HER	Units
Beam energy	3.5	8	4	7	GeV
Beam current	2	1.4	3.6	2.6	A
Bending radius	85.7	580	177.4	580	m
SR power	48	136	72	149	W/mrad

will use source bends in the same locations as at KEKB, which are the 5 mrad ???weak bends??? heading into the Fuji (LER) and Oho (HER) straight sections. At SuperKEKB, the beam currents will be higher, as shown in Table 9.12. The source bend for the LER will be replaced with one with a longer core and larger bending radius (a re-used LER regular arc bend magnet) in order to reduce the SR power intensity. Despite the reduced bending radius, the increase in beam energy and beam current means that the incident angular power density will be higher (72 W/mrad) than that of the KEKB LER (48 W/mrad). The source bend will remain the same at the HER, and the effect of the increased current of the beam is almost cancelled out by the reduced beam energy, so that the angular power density is only a little bit higher than at KEKB.

It is planned to move the chambers a bit further downstream from the source bends than they were at KEKB, which will help reduce the SR power intensity hitting the primary extraction mirrors. However, the heat deformation of the KEKB mirrors was already a very significant problem, requiring complicated measures to measure and compensate for the distortion in real time in order to correct the beam-current dependence on the measured beam size. For this reason, we are planning to use mirrors made of diamond[2]. The superior thermal conductivity and low thermal expansion coefficient of diamond is expected to make the the apparent change in magnification at full current much lower than was seen with the beryllium mirrors at KEKB.

The design of the mirror is based on CVD diamond, made by Cornes Technology and EDP Corporation. For best thermal conductivity, the ideal mirror material would be a pure monocrystalline diamond, rather than a polycrystalline one. The mirrors that have been fabricated for initial use at SuperKEKB consist of 3 monocrystalline segments, each approximately 9 mm x 9 mm, joined together to make a 9 mm x 28 mm rectangle, 0.8

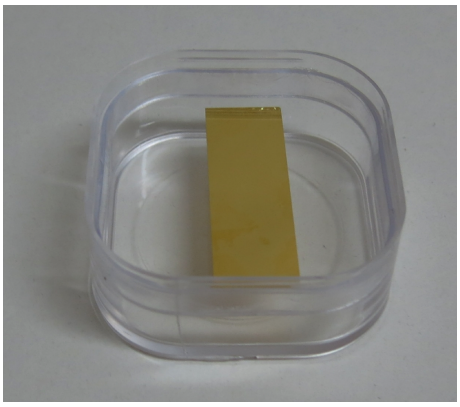

Figure 9.38: Gold-coated diamond mirror for SuperKEKB visible SR monitor.

mm thick. For optical reflectivity, a metallic surface is needed. A 1 μm Au reflective surface is bonded to the diamond substrate with a Cr bonding layer between the gold and diamond. An example of one of the produced mirrors is shown in Figure 9.38. The monocrystalline diamond also gives good surface smoothness after polishing; production samples show Ra values between 1.1 and 7 nm.

ANSYS simulations showed that for any holder design which touches the mirror on all edges or along the back side, the deformation of the holder would be large enough to cause unacceptable deformations in the surface of the diamond mirror, much larger than the deformations caused by the heat distribution pattern in the diamond mirror itself. The holder design that has been adopted is a split cylinder of soft copper, which grips the mirror near one edge only. The soft copper permits good heat-sinking contact with the portion of the mirror surface gripped within the split (about 5 mm), without placing extraneous strain on the surface of the mirror due to heat deformation of the copper. The holder is shown in Figure 9.39.

The mirror is set inside a 24 mm-high antechamber, as shown in Figure 9.40, to minimize HOM losses. The loss factor for the mounted mirror assembly is calculated using GdfidL to be 0.8×10^{-6} V/pC, which correspond to an expected loss of 41 mW at full current in the LER.

The visible-light SR monitor will start commissioning from Phase I.

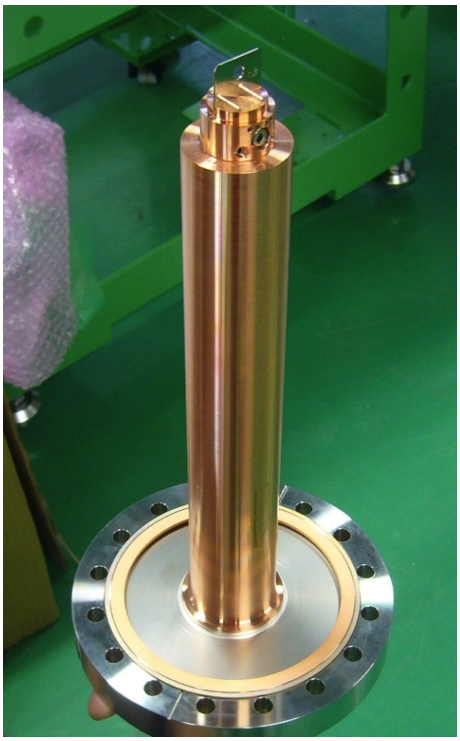

Figure 9.39: Heat-sinking holder for diamond mirror. A metallic dummy plate (with hole in it) is inserted in place of the mirror. Actual mirror has no hole in it.

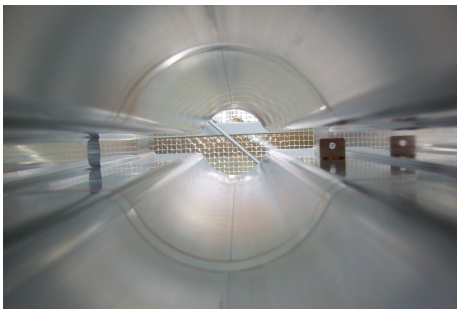

Figure 9.40: SR extraction chamber with metallic dummy plate (with hole in it) inserted in place of the mirror. Actual mirror has no hole in it. (Extraction chamber design by Y. Suetsugu, vacuum group.)

9.4.2 X-ray beam profile monitor

Overview

X-ray beam profile monitors are being installed in each ring to provide high-resolution bunch-by-bunch, turn-by-turn measurement capability for low-emittance tuning, collision tuning, and instability measurements. Two sets of optics will be installed, one a simple pinhole (single-slit) type, and the other a coded aperture. Coded aperture imaging is a technique originally developed by X-ray astronomers[3], using a pattern mask to modulate the incoming light. The projected image on the detector is then decoded using the known mask pattern to reconstruct the original image. The large open aperture provides much higher photon throughput than a single pinhole, allowing better photon statistics-limited resolution in single-shot measurements. Research and development of the monitors has been carried out in collaboration with Cornell University, University of Hawaii and SLAC. Beam size measurements using coded apertures down to ≈ 10 μm have been demonstrated at the CesrTA accelerator at Cornell[4].

Beam lines and heat load

The X-ray sources are the last arc-bends located immediately upstream of the straight sections in Fuji (LER) and Oho (HER). The final LER arc bend for SuperKEKB has been split into two re-used KEKB arc bends, with the x-ray source point being located in the upstream half of the pair. This provides more x-ray flux for the LER monitor than would have been received from one of the new SuperKEKB LER arc bends.

The parameters for the beamlines are shown in Table 9.13. The beam lines are about 40 meters long from the source points to the detectors. The optical elements (pinhole, coded aperture) are located in optics boxes $\approx 9-10$ meters from the source point, for geometrical magnification factors of $\approx 3\times$ for both lines.

The beam lines are connected directly to the ring vacuums. Gate valves will be located upstream of the optics boxes for isolation when opening the optics boxes or doing other vacuum work downstream on the beam lines, or in the event of a vacuum leak downstream. Insertable beam stoppers will be located directly upstream of the gate valves to protect them from the high incident SR power when needed.

The incident power density on the optics boxes with no filters are 23 and

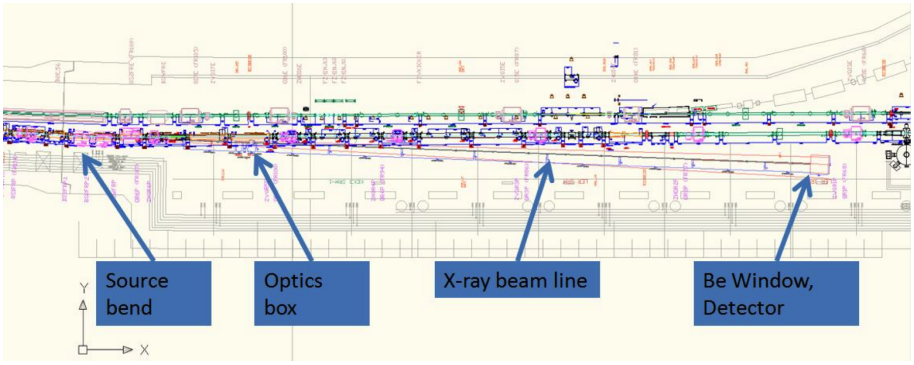

Figure 9.41: Location of x-ray monitor beam line for the LER in the Fuji straight section.

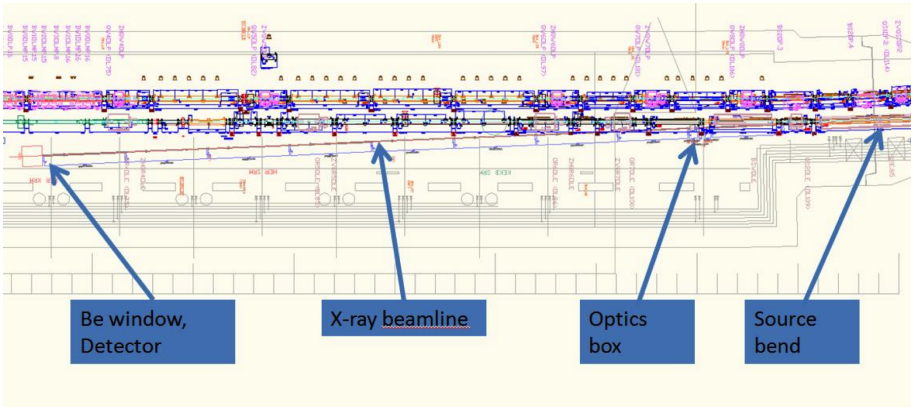

Figure 9.42: Location of x-ray monitor beam line for the HER in the Fuji straight section.

Table 9.13: X-ray monitor beam line parameters.

Parameter	LER	HER	Units
Vertical beam size σ_y at source point	20	11	μm
Beam energy	4	7	GeV
Source bend radius ρ	31.74	106	m
Critical energy	4.4	7.1	keV
Zero-degree source SR power density	0.56	2.8	kW/mrad^2/A
Distance from source to optic	9.39	10.27	m
Beam current	3.6	2.6	A
Incident power density on optic (w/no filter)	23	69	W/mm^2
Distance from source to detector	40.7	42.55	m
Be extraction window thickness	200	200	μm
Power density on detector (w/no filter, optics out)	0.7	2.8	W/mm^2

69 W/mm^2 for the LER and HER, respectively. The optics elements consist of $\approx$ 20 μm thick gold masking material on silicon or diamond substrates. High-power tests carried out at CesrTA[5] indicate that silicon-substrate x-ray optics elements can just tolerate the LER power density, but with very little margin. The diamond-substrate mask is more robust (due to the better hear-conduction of diamond over silicon), so has more margin available. A Be filter may be used upstream in the LER to bring incident power levels down a bit further, though this would come at the expense of photon flux. In the HER, upstream Be filters are required to bring the incident power level down to that of the LER line. The Be filters will be placed upstream of the stoppers. Further upstream of the Be filters will be 4 mm-wide collimators, to block unnecessary off-axis x-ray power from hitting the beam pipe walls.

Screen monitors will be installed on the downstream sides of the beam-lines, midway between the optics boxes and detectors, to aid in final, x-ray beam-based alignment.

Detector and read-out

A one-dimensional pixel array will be used, primarily for vertical beam size measurements. An InGaAs array with 50 μm pitch has been used at CesrTA, and it is very efficient for low-energy x-rays (up to a few keV). A similar array

has been prepared for SuperKEKB, but its efficiency for x-ray detection drops off at higher energies, due to the thinness of the sensing element (about 3.5 μm deep). In order to detect more efficiently x-rays in the 10-20 keV range, where the SuperKEKB spectrum peaks after passage through beam line elements, a novel type of detector is under development at SLAC for use at SuperKEKB. This detector is made of a silicon wafer mounted edge-on to the beam, providing a sensing depth of 2 mm, which is enough to absorb 90% of the incident spectrum expected. The high collection efficiency will improve the statistical resolution for single-shot measurements. Readout traces run parallel to the beam direction, so that electron-hole pairs created anywhere along the sensing depth can be read out rapidly. The thickness of the wafer in the direction perpendicular to the beam is 75 μm. Simulations show that the tails of the current time distribution fall off within 2 ns at a 200 V bias voltage, sufficient for good bunch-to-bunch separation. (The rise time of the charge pulse is a few tens of ps, which may potentially open up possibilities for crude longitudinal diagnostics for head-tail instability studies, depending on the coupling characteristics of the readout.)

A layout diagram of the detector strip design in fabrication at SLAC is shown on the left in Figure 9.43. The collection efficiency can be improved further by stacking detector strips perpendicular to the beam axis and ganging corresponding pixels of parallel strips together; the strip on the right in the figure is designed for easy stacking with the strip on the left. Both strips comprise 128 traces at 50 μm spacing. This spacing was chosen based on simulations of the statistical resolution achievable with various candidate optics patterns as a function of detector pixel size. Charge blooming within the detector is expected to be about 2-4 μm, based on CASINO[6] simulations.

A high detection efficiency implies a high absorbed heat load. It is planned to mount the detector strips on monocrystalline diamond heatsinks (similar to the ones used for the mask substrates). Calculations of the detectable spectra using this detector are shown in Figure 9.44.

The digitizing and read-out electronics are being developed at the University of Hawaii, based on high-speed read-out systems developed there for high-energy physics detectors. A 64-channel development motherboard is shown in Figure 9.45. It features interchangeable daughter cards for use with different digitizer ASICs. Two such custom ASICs have been developed so far, one optimized for reading out a few bunches (or bunch slices) over many turns, and one for reading out all bunches over a few turns. Further ASIC development is expected as familiarity with the current ones is devel-

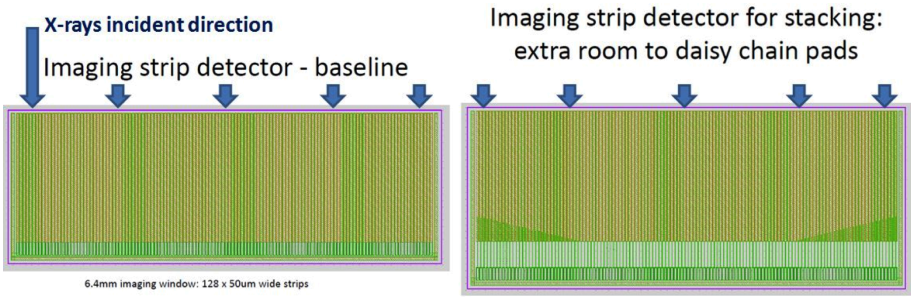

Figure 9.43: High-energy x-ray detector layout. Left: Primary detector strip layout. Right: Secondary detector strip for stacking in parallel with primary detector strip.

oped, and as needs evolve. Full 128-channel readout is also planned for the future.

To analyze the data, a template-fitting procedure has been developed for analysis of CesrTA data. A 64-CPU analysis computer will be dedicated to each beam line for performing rapid fitting of the x-ray monitor data, with results to be written to the EPICS database for machine tuning purposes.

Optics and resolution

The single-shot resolution of the x-ray monitor at low intensities is dominated by photon statistics. The resolutions given by different mask patterns have been evaluated by calculating the distinguishability between the images seen by the detector for beams of different sizes. An approach similar to that described in Ref. [7] has been used to calculate the suitability of different x-ray optic (mask) patterns at different beam sizes.

Figure 9.46 shows, on the left, the simulated detector images for a 32 μm pinhole (slit) pattern, assuming gold masking on a diamond substrate and the high-energy detector under development, at the SuperKEKB LER. On the right are the resolution contours for a range of beam sizes, where different colors denote different bunch currents. The inner, light-blue contours correspond to full beam current, and the outer, red ones correspond to 1/128th beam current (equivalent to the typical beam currents used for machine optics correction). While the single pinhole is in some ways the easiest one to analyze, it is not expected to be useful for single-shot measurements during

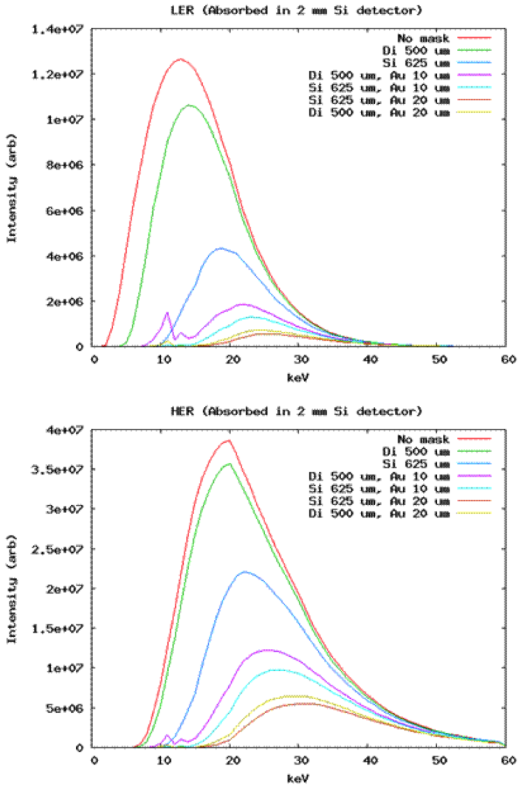

Figure 9.44: Calculations of x-ray spectra detectable with high-energy detector for raw beam and various types of optics. Left: LER, assuming 200 μm Be extraction window. Right: HER, assuming 200 μm Be extraction window and 1.4 cm Be filter upstream.

Figure 9.45: 64-channel motherboard for development, with digitizer daughter cards.

standard optics correction modes, unless the beam current is concentrated in a small number of bunches.

For better resolution, it is planned to use a coded aperture pattern. The coded aperture pattern used at CesrTA is a Uniformly Redundant Array (URA)[8], which features an open aperture of 50% with an even sampling of spatial frequencies in the non-diffractive limit. An example of a candidate URA mask for use at SuperKEKB is shown in Figure 9.47. It is a 59-element (where each element can be filled or not) URA mask pattern with minimum feature size of 10 μm, and is thus 590 μm in height.

The simulated detector images and resolution contours for the URA pattern are shown in Figure 9.48. The resolutions at low beam currents are significantly better than those for the single pinhole. As mentioned above, this is due to the greater open aperture, leading to greater detected photon flux, as well as the presence of beam size-dependent modulation depths.

Other patterns are currently under investigation as well. Figure 9.49 shows the results for one recently developed pattern being considered that uses 32 μm pinholes in a logarithmically distributed range of spacings, designed to provide good resolution over a range of beam sizes. This pattern clearly improves on the resolution of the URA pattern.

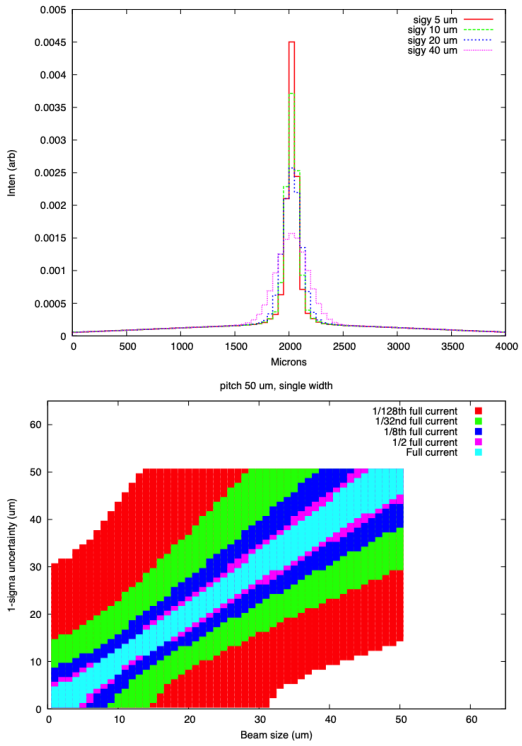

Figure 9.46: Left: Simulated detector images for different beam sizes using 32-micron pinhole and 50 micron pitch deep silicon detector at LER. Right: Single-shot statistical resolution contour plots for the same combination.

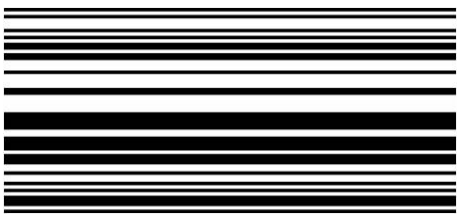

Figure 9.47: 59-element URA mask pattern for SuperKEKB.

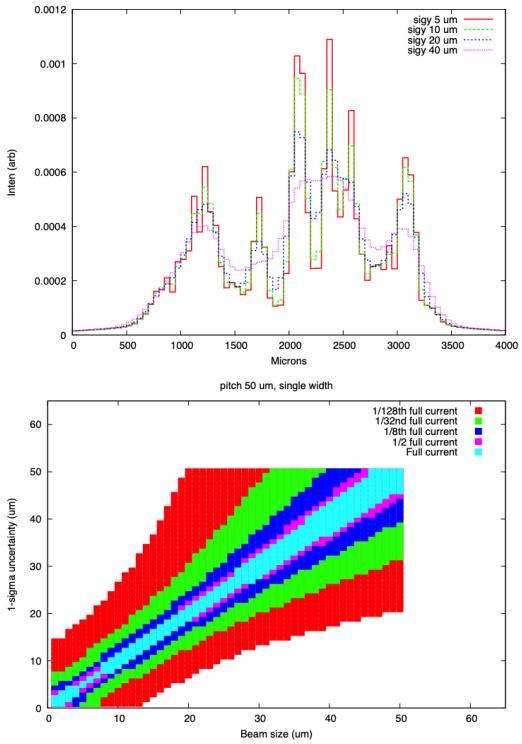

Figure 9.48: Left: Simulated detector images for different beam sizes using URA mask pattern and 50 micron pitch deep silicon detector at LER. Right: Single-shot statistical resolution contour plots for the same combination.

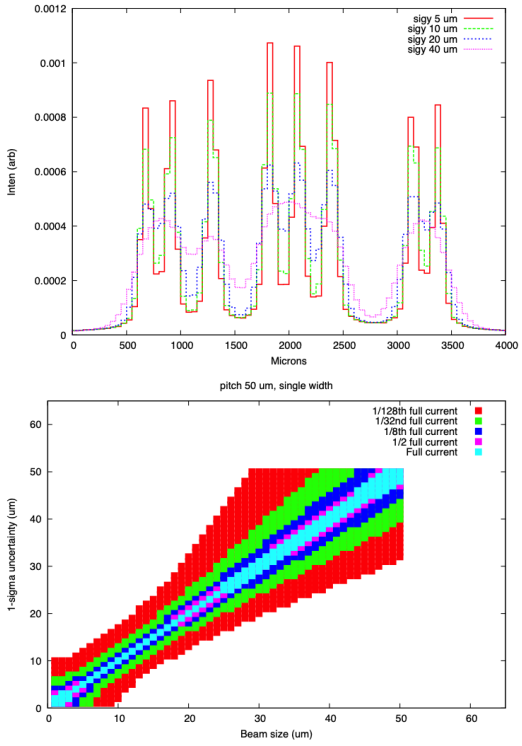

Figure 9.49: Left: Simulated detector images for different beam sizes using multiple 32-micron pinhole pattern and 50 micron pitch deep silicon detector at LER. Right: Single-shot statistical resolution contour plots for the same combination.

The x-ray monitor will start commissioning from Phase I, for use as soon as possible for low-emittance tuning.

9.4.3 Large Angle Beamstrahlung Monitor

We have a plan to install a Large Angle Beamstrahlung Monitor (LABM), originally developed by G. Bonvicini of Wayne State U. for use at CESR. Beamstrahlung is light generated by the beam-beam collision, as the particles in each beam are deflected by the opposing beam, similar in principle to synchrotron radiation. Like synchrotron radiation, the resulting beamstrahlung light is polarized in different axes depending on the direction of deflection of each particle. The monitor does not measure beam sizes directly, but uses the relative strengths of horizontal and vertical polarization components of large-angle ($\approx$ 10 mrad off-axis) beamstrahlung to diagnose the quality of collisions, allowing the evaluation of parameters such as beam separation and relative beam sizes at the collision point, as shown schematically in Figure 9.50. Estimation of signal and background level shows that a much stronger signal than that seen at CESR is expected at SuperKEKB.

To extract the light, two pairs of mirrors are installed, one on either side of the IR. One mirror on each side is mounted on the upper wall of the IR chamber, and reflects the light out of an extraction port on the lower wall. The other mirror on each side is mounted on the lower wall, reflecting upwards. The four sets of extracted beamstrahlung light are then transferred by a series of mirrors to optics boxes mounted at the Tsukuba B4 level below the accelerator beam line, and directed into optics boxes (see Figure 9.51). The light from each beam is split into vertical and horizontal polarization components via a Wollaston prism, then further divided into 4 wavelength bands, with the intensity of light in each polarization and wavelength combination being measured by PMTs.

The Be extraction mirror and extraction chamber design design are shown in Figure 9.52. The front face of the mirror, at a 45-degree angle, is 2 mm wide, and extends 2 mm in height and in longitudinal extent, with a shallower-sloped trailing edge. The extraction mirror is set within a slotted ramp structure, which shields the mirror from electric fields generated by the passing beam. The ramp is 6 mm in height around the mirror, with 30-degree sloped leading and trailing edges. The mirror sits inside a 3 mm-wide slot. GdfidL calculations give a loss factor of 12.3×10^{-3} V/pC for each chamber, which will generate about 645 W at full LER current, with the

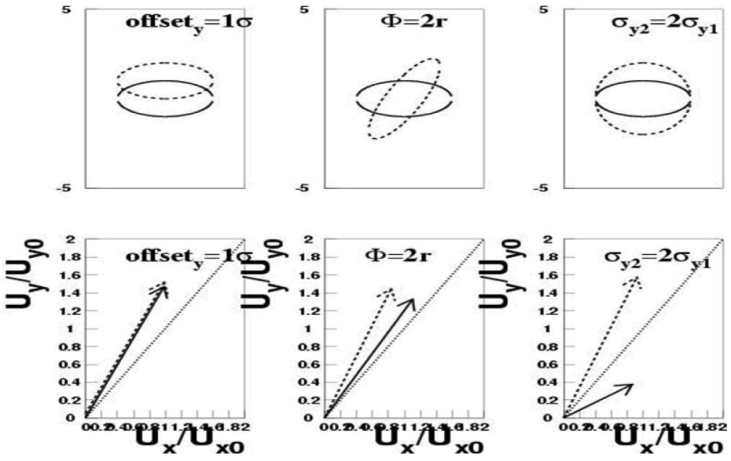

Figure 9.50: Example of collision mismatch diagnosis using x- and y-polarization components. Upper plots represent, from left to right: offset, tilt and size mismatches between the two colliding beams. Lower plots show the corresponding shifts in measured polarization vectors (x-axis = normalized x-polarization; y-axis = normalized y-polarization component).

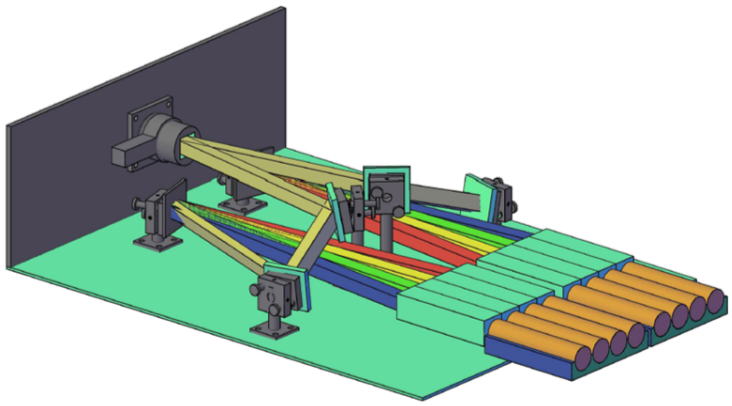

Figure 9.51: Design of optics box that splits beamstrahlung light into different polarization components and wavelengths for measurement by PMTs.

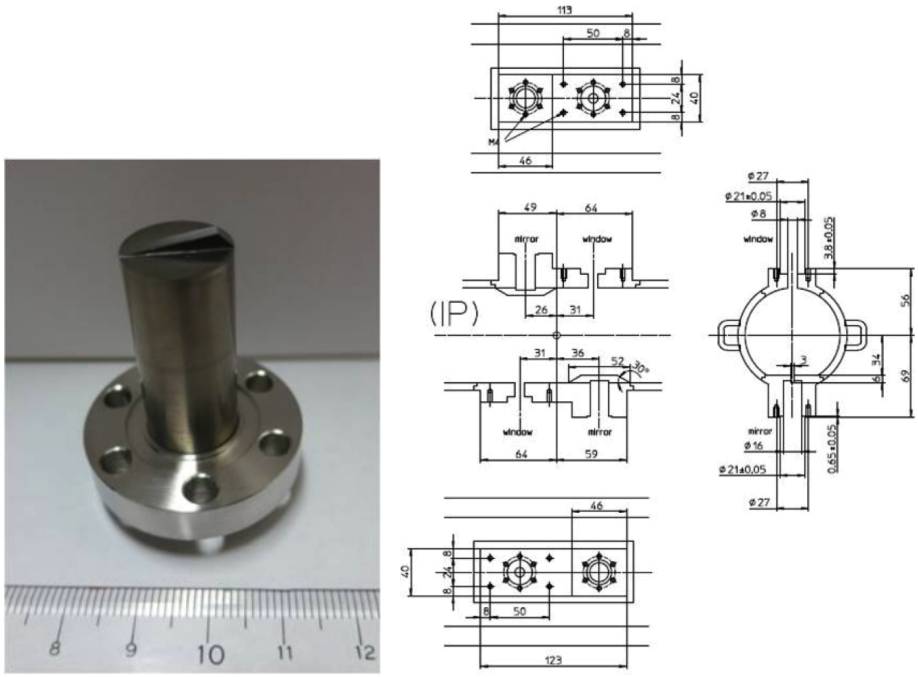

Figure 9.52: Left: Be extraction mirror for LABM. Right: Extraction mirror chamber design (by K. Kanazawa, vacuum group).

majority of that due to the shield ramps, and only a few Watts due to the 8 mm-wide extraction window holes. Very little field leakage into the mirror area is found.

The LABM will begin initial commissioning and background studies in Phase I, when there will be no background from the QCS quadrupoles magnets. If beams can be collided at some point in Phase I, even at extremely low luminosity, that would provide valuable data for systematic studies.

Bibliography

[1] M. Arinaga, J. Flanagan, S. Hiramatsu, T. Ieiri, H. Ikeda, H. Ishii, E. Kikutani , T. Mimashi, T. Mitsuhashi, H. Mizuno, K. Mori, M. Tejima and M. Tobiyama Nucl. Instrum. Meth. Phys. Res. **A499**, p100-137, (2003).

[2] J.W. Flanagan, M. Arinaga, H. Fukuma, H. Ikeda, "Diamond mirrors for the SuperKEKB synchrotron radiation monitor," Proc. IBIC12 , Tsukuba (2012).

[3] R.H. Dicke, Astrophys. Journ., **153**, L101, (1968).

[4] J.P Alexander, A. Chatterjee, C. Connolly, M.P. Ehrlichman, E. Fontes, B.K. Heltsley, W. Hopkins, A. Lyndaker, D.P. Peterson, N.T. Rider, D.L. Rubin, J. Savino, R. Seeley, J. Shanks, J.W. Flanagan Nucl. Instrum. Meth. Phys. Res. **A748**, p96-125, (2014).

[5] J.W. Flanagan, M. Arinaga, H. Fukuma, H. Ikeda, A. Lyndaker, D.P. Peterson and N. Rider, "High-power tests at CesrTA of x-ray optics elements for SuperKEKB,"Proc. IBIC13, Oxford (2013).

[6] Drouin, D., Couture, A. R., Joly, D., Tastet, X., Aimez, V. and Gauvin, R. "CASINO V2.42???A Fast and Easy-to-use Modeling Tool for Scanning Electron Microscopy and Microanalysis Users," Scanning, 29: 92???101 (2007).

[7] J.W. Flanagan, M. Arinaga, H. Fukuma, H. Ikeda, T. Mitsuhashi, J.S. Alexander, M.A. Palmer, D.P. Peterson, N. Rider, G. Varner "SINGLE-SHOT RESOLUTION OF X-RAY MONITOR USING CODED APERTURE IMAGING," Proc. DIPAC11, Hamburg (2011).

[8] E.E. Fenimore and T.M. Cannon, Appl. Optics, V17, No. 3, p. 337 (1978).

9.5 Other instrumentations

9.5.1 Beam loss monitors

Beam loss monitor (BLM) system is used for the protection of accelerator components against unexpected beam loss caused by, for example, beam instabilities. An interlock signal from a BLM triggers a beam abort. We will use the same BLM system as that in KEKB [1] that consists of ion chambers and PIN photo-diodes. The number of channels of BLM is approximately 200. We use data loggers to diagnose whether the abort is correctly requested by BLM and other sensors or not.

Ion Chamber

Ion chambers which are shown in Fig. 9.53 are re-used sensors of KEKB. The 5m long chambers are mounted on cable racks located on the outer wall along the tunnel. The ion chamber is a Fujikura FC-20D co-axial cable. The inner and outer conductors are separated by an air gap. The applied voltage at outer conductor is 200V. The typical drift time where the positive ions are reached at inner conductor is 1ms. The resulting current is sent to readout electronics which includes an integrator and an amplifier as shown in Fig. 9.54. Each module handles eight channels. The amplifier gain can be selected to 1, 10 or 100. The RC time constant also can be selected to 10, 100, 300 or 1000ms. The beam abort is requested when the beam loss level exceeds a threshold that is set for individual channel. The loss signal is buffered and sent to a 16-bit, 64 channel ADC (DGX 18K14B) and logged with 1Hz. The same signal is sent to the data logger with high-sampling-rate immediately after the beam abort.

PIN photo-diode

Collimators are installed in beam line in order to protect the Belle-II detectors from the beam. The number of the collimators is 13 and 16 in LER and HER respectively. High current beam may damage the collimator itself when the beam orbit changes rapidly. PIN photo-diodes (PDs) are used as sensors of

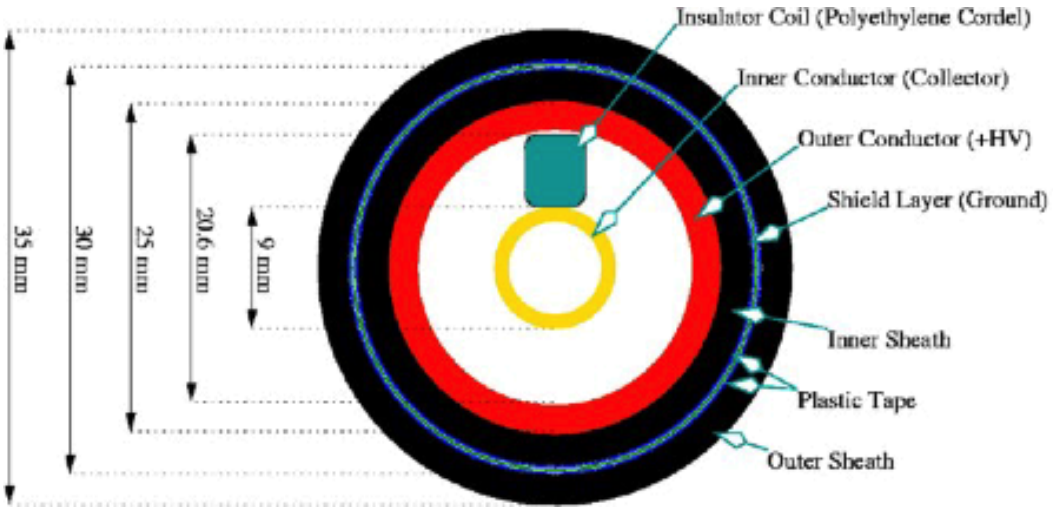

Figure 9.53: Ion chamber for the beam loss monitor[1].

the BLM at the collimators since the interlock signal from the ion chamber is not fast enough to protect the collimators. The rise time of PD is 60 μs which is determined by the capacitance of the signal cable (30nF for a 400m cable) and an input resistance of 2kΩ of the readout electronics. The readout electronics is a modified ion chamber readout that has a track-and-hold circuit as shown in Fig. 9.55. The interlock signal is asserted within a few turns after beam loss happened. The PIN signal can protect the hardware from the localized and rapid beam loss, and be used to distinguish the ring where the beam loss occurred. Therefore we install PINs to several places where we expect the localized beam loss besides the collimators as shown in Fig. 9.56. The signal flow after the readout module is same as that of the ion chamber signal.

Data logger system

The diagnostic system of the beam abort is based on a high-sampling-rate data logger that records BLM and other signals at the moment of the beam abort [9]. BLM signals of all over the rings are collected to four local control rooms (LCRs). The data loggers are located in five LCRs where the BLM signals and signals from RF cavities are corrected. The logged time period is 600 ms or 300 ms. Sampling intervals are 5 μs or 1 μs depending on the

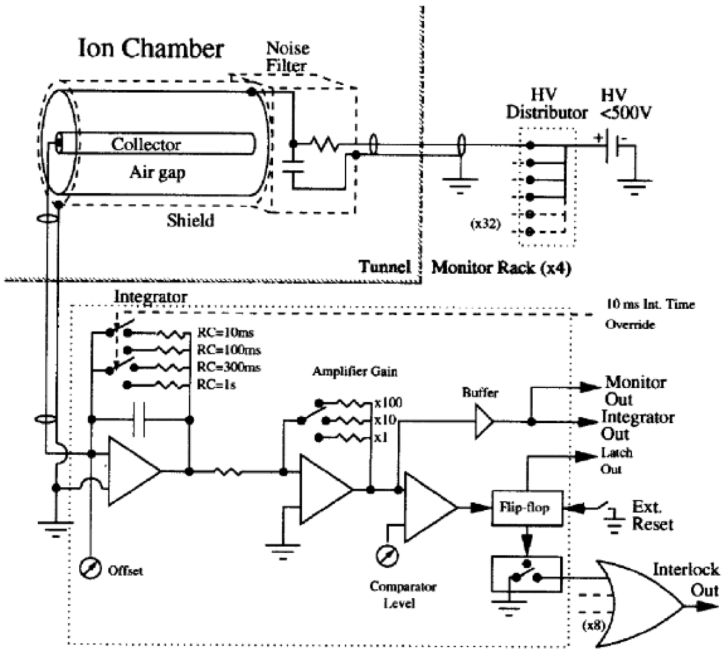

Figure 9.54: Block diagram of the read-out electronics for the ion chambers[1].

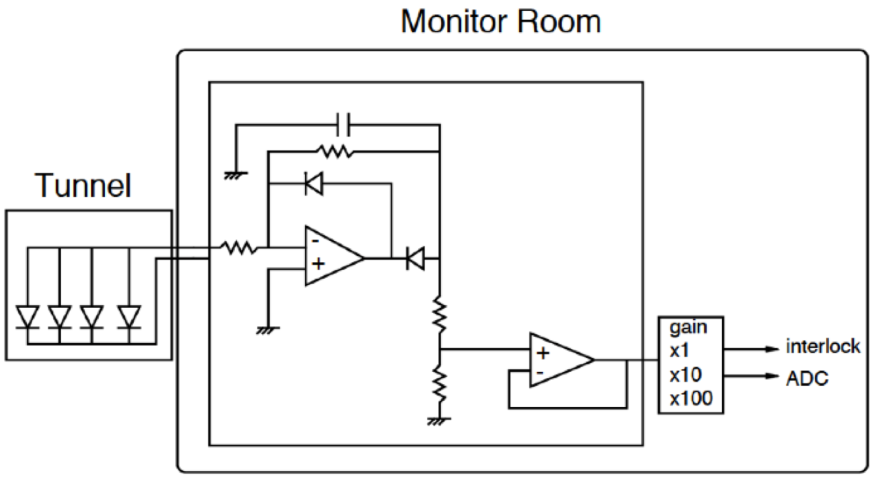

Figure 9.55: Block diagram of the read-out electronics for the PIN photodiodes[1].

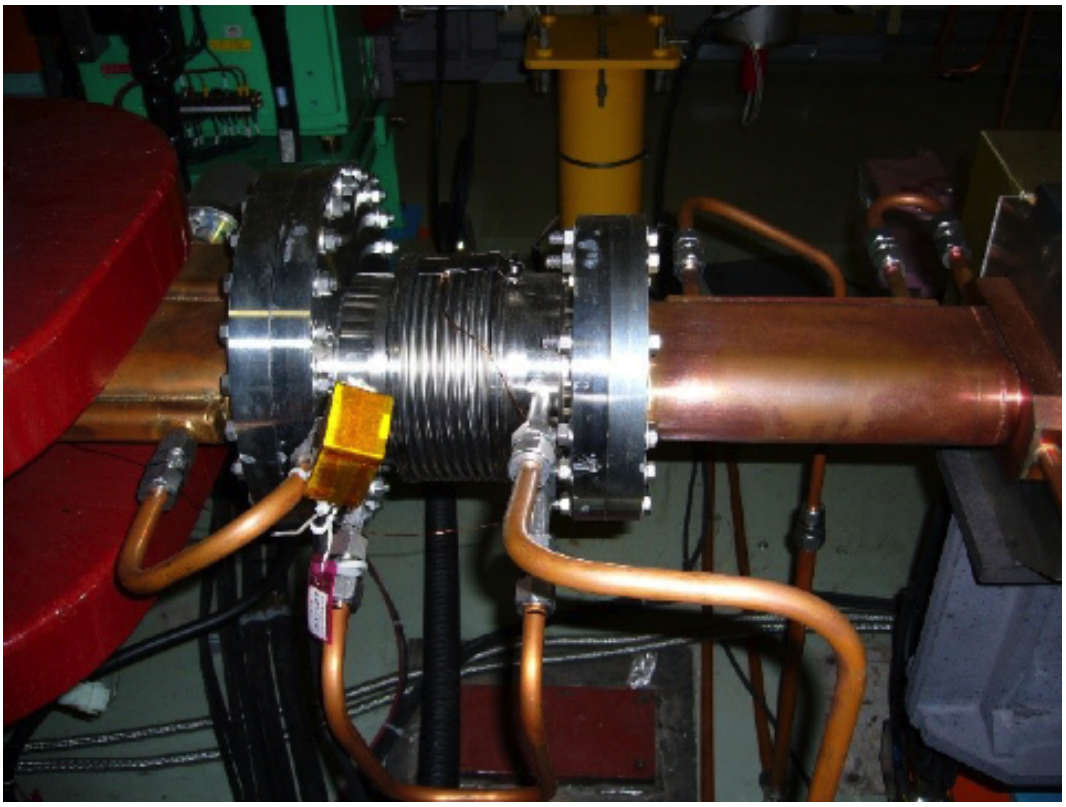

Figure 9.56: An example of PIN photo-diodes which are put near bellows.

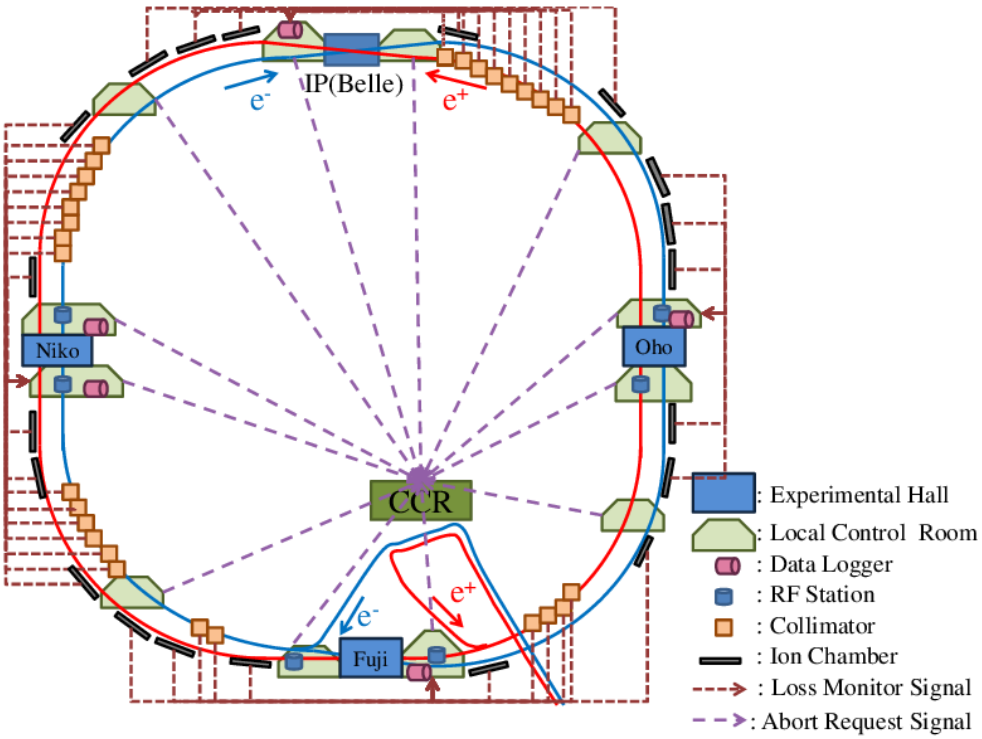

Figure 9.57: A signal flow of data loggers[2].

logged time periods of 600 ms or 300 ms respectively. The signal flow is shown in Fig. 9.57. Beam intensity, signals from the RF cavities and beam phase showing deviation of synchronous phase from the timing signal of injection trigger are logged with a part of BLM signals. These fast signals are useful to diagnose the cause of the beam abort. The recorded data are sent to the central control room (CCR) via the KEK internal network. The information is ready for inspection within a few minutes after the abort. Analyzing the data, the reason of beam loss and the beam abort is identified and the best condition of the beam abort is determined.

9.5.2 DCCT and CT

In SuperKEKB we will use the same DCCT and CT systems as those used in KEKB[1, 2] except for the DCCT circuit in LER whose maximum range of

$\sim$ 3 A exceeds the design beam current of SuperKEKB LER. We will modify it to accept the beam current up to 5 A. Location of the DCCT and CT in LER will be slightly moved due to change in positron injection system.

The measurement system will be slightly modified to realize faster measurement of the beam current and beam lifetime. Employing the Agilent 34410A fast digital volt meter, we plan to measure the beam current at the sampling rate of 5k samples per second with the resolution of about 16 bit. The average beam current, average injection rate and fitted lifetime will be calculated on a Linux IOC to update the data once per second. R&D of such a system is in progress.

Bibliography

[1] M. Arinaga, J. Flanagan, S. Hiramatsu, T. Ieiri, H. Ikeda, H. Ishii, E. Kikutani , T. Mimashi, T. Mitsuhashi, H. Mizuno, K. Mori, M. Tejima and M. Tobiyama Nucl. Instrum. Meth. Phys. Res. **A499**, p100-137, (2003).

[2] Mitsuhiro Arinaga, John W. Flanagan, Hitoshi Fukuma, Takaaki Furuya, Shigenori Hiramatsu, Hitomi Ikeda, Hitoshi Ishii, Eiji Kikutani, Toshiyuki Mitsuhashi, Kenji Mori, Masaki Tejima, and Makoto Tobiyama, Prog. Theor. Exp. Phys. (2013) 03A007.